Utrecht University

Debye Institute for Nanomaterials Science

Master Thesis

Resolving Oil-to-Water Channel Leakage in Bijels

On the Road to a 3D Janus Porous Material

Jelle Martijn Prinsen

Graduate School of Natural Sciences

Physical Colloid Chemistry

Debye Institute for Nanomaterials Science

Utrecht University

February 21st, 2022

Supervisors:

M.A. Khan

Dr. M.F. Haase

Abstract

Hydrogen fuel cells are essential in the transition to sustainable electricity, since the output of renewable energy sources fluctuates over time. The conversion from chemical to electrical energy is performed by a proton-exchange membrane fuel cell (PEMFC). PEMFCs suffer from lowered efficiency due to water flooding, which hinders the diffusion of the oxygen reactant at the cathode. Hydrophilic and hydrophobic regions in the gas diffusion layer (GDL) improve the mass transport of these two chemicals. A bicontinuous interfacially jammed emulsion gel (bijel) offers two interwoven, fully continuous pore systems of oil and water. Our goal is to phase-selectively hydrophobize the bijel scaffold to create a Janus porous medium, which could serve as a GDL. The hydrophobized channel network facilitates oxygen diffusion, while the untreated pores remain hydrophilic and allow for the transport of water. Bijels are promising candidates to become the first material to extend the asymmetric Janus character to 3 dimensions. *Solvent Transfer-Induced Phase Separation* (STrIPS) is used for the continuous fabrication of bijel-based templates with sub-micron domains. The system is characterized with scanning electron microscopy (SEM) and confocal microscopy. The present work shows that the hydrophobic character of the particles causes any oil to leak into the water channel. The rate of flooding depends on the oil viscosity. Consequently, the loss of phase-distinction inhibits phase-selective hydrophobization. The removal of oil residue and surfactant from the aqueous phase via electro-osmosis is a promising solution to circumvent the structural degradation which impedes the fabrication of Janus bijels. The application of bijels into a Janus porous GDL would raise the efficiency of mass transport and thereby increase the power density of hydrogen fuel cells.

Table of Contents

Glossary

Bicontinuous

One network consist of a whole, single unit, which is interwoven with another fully continuous network

Colloidal particle

Particle with a diameter in the 1-1000 nm range

Contact angle

The angle between phases. For interfacial particles this is measured between the water-fluid and water-particle interfaces, by convention.

Domain size

The pore length in porous materials

Janus particle

Particle with opposing characteristics on either side, such as charge, composition or polarity

Neutrally wetting particle

Particle with a contact angle of 90° at a liquid-liquid interface

Pickering emulsion

Emulsion stabilized not by surfactants, but by interfacial solid particles

Radial channel

A radially aligned cavity inside the water channel of bijels

Radial pore size gradient

Variation in domain size across the radial dimension of bijel fibers

Small-domain bijel

Bijel with pore size below 5 µm

List of Abbreviations

bijel	bicontinuous interfacially-jammed emulsion gel
CTAB	cetrimonium bromide
DEP	diethyl phthalate
GDL	gas diffusion layer
HTES	n-hexyltriethoxysilane
ID	inner diameter
O/W	oil-in-water
OD	outer diameter
OTS	n-octadecyltrichlorosilane
Pe	Peclet number
PEMFC	proton-exchange membrane fuel cells
Re	Reynolds number
RI	refractive index
ROI	region of interest
SEM	scanning electron microscopy
STrIPS	Solvent Transfer-Induced Phase Separation
TEOS	tetraethyl orthosilicate
UV	ultra-violet
w	weight fraction
W/O	water-in-oil
wt.%	weight percentage
θ	contact angle of colloid at an interface
ϕ	volume fraction

1. Introduction

While European countries currently only get 20% of their electricity from renewable sources,[1] the EU aims to be climate neutral by 2050.[2] Problematically, a fully sustainable electrical grid would suffer from fluctuations in natural energy resources (**Figure 1**).[3] Therefore, buffers are needed to ensure energy demand can be matched. During moments of excess production, green electricity could be used to hydrolyze water. The formed hydrogen can later be used in a *proton-exchange membrane fuel cell* (**PEMFC**) as a carbon free solution to meet the demand in electricity.[4] At the anode of such a device, hydrogen is split into protons and electrons. Electricity is generated because the membrane is only permeable to protons, and the electrons are forced through an electrical network. At the cathode, these particles combine with oxygen to form water.[5] The produced water should be removed, as it limits the supply of the reactant oxygen to the electrode.[6] The porous gas diffusion layer (**GDL**) provides flow channels for the diffusion of oxygen and water.[7] State-of-the-art GDLs contain hydrophilic regions which facilitate aqueous mass transport, and hydrophobic sections for oxygen diffusion.[8] The regulation of diffusion routes prevents tortuous paths which impede mass transport and lower the power output of the PEMFC. Finally, wide pores in GDLs can fill with water regardless of their hydrophobic character.[9] Therefore, a material with separated, microscopic pore systems would increase the power density of PEMFCs.

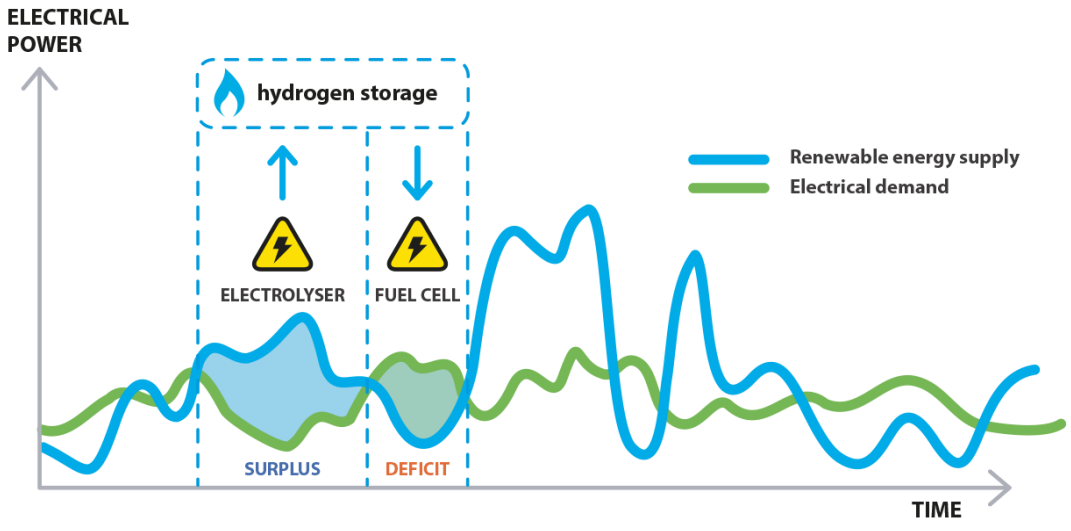

Figure 1: Electrolysis converts excess electricity to hydrogen, which can be used in hydrogen fuel cells to meet the electrical demand. Adapted with permission, Copyright Hydron Energy B.V.

A *bicontinuous interfacially jammed emulsion gel* (**bijel**) is such a material which consists of two highly intertwined microstructured pore systems (**Figure 2**a).[10] Moreover, bijel-templated materials have already been found to increase mass transport efficiency because of the highly connected and unconstructed channels.[11] The arrangement would allow for separated transport of water and oxygen, which makes bijels promising templates for gas diffusion layers in PEMFCs (Figure 2b).

There are multiple fabrication routes to bijels, most of which rely on the demixing of initially miscible liquids.[12] Where nucleation results in isolated droplets, spinodal decomposition forms the desired bicontinuous arrangement. Because of the absence of a thermodynamic barrier in the latter, demixing occurs spontaneously throughout the entire liquid.[13] Over time, the domains become larger as the system minimizes the interfacial area, a process known as *coarsening*. Solid particles can arrest the phase-separation process via interfacial jamming. These particles should be neutrally wetting in order to allow the interface to curve towards both substituents.[14]

Although most fabrication procedures rely on batch processes, *Solvent Transfer Induced Phase Separation* (**STrIPS**) allows for the continuous fabrication of bijel fibers.[15] The removal of solvent from a ternary mixture leads to an increase in the interfacial tension. Additionally, the solubility of the surfactant *cetrimonium bromide* (**CTAB**) decreases, which induces the *in-situ* particle modification via electrostatic adsorption of CTAB to the surface.[16] The decomposition is arrested once the particles become neutrally wetting at a sufficiently high interfacial tension. Therefore, more rapid solvent diffusion from the ternary mixture leads to earlier arrest of the coarsening process, and smaller domains. We subsequently apply a number of post-processing techniques on the fabricated bijel fibers.

Importantly, lipophilic dyes only enter the oil channel (Figure 2d), which shows that the oil channel in the bijel opens to the ambient phase.[17] Analogously, we hypothesize that oil-soluble reagents also only diffuse into the oil channel. Our aim is to use lipophilic silane reagents to hydrophobize only the walls of the oil phase. Consequently, we use trichloro- and triethoxy alkylsilanes with long hydrocarbon substituents to covalently modify the particle surface. We expect that chlorosilanes react more readily than ethoxysilanes.[18] The phase-selective hydrophobization would leave the other channel unaltered, which would remain hydrophilic due to the hydroxyl groups at the particle surface (Figure 2c). Lastly, the fragile bijel structure needs to be strengthened before it can be used as a GDL. Bijels collapse upon drying due to the

absence of an oil-water interface. This problem is resolved via the deposition of silica by *tetraethylorthosilicate*(**TEOS**), which crosslinks the nanoparticles.[19]

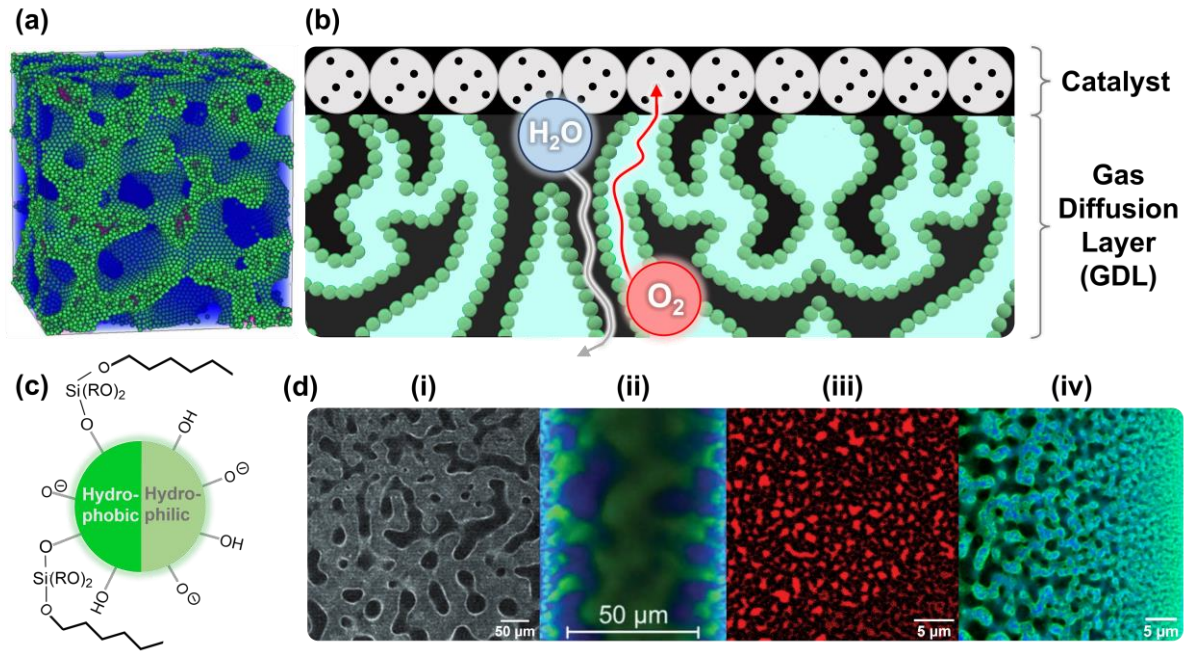

Figure 2: (a) 3D reconstruction of a bijel; phase A in blue, phase B in red, particles in green. Adapted with permission from ref. 20. Copyright Elsevier (2015). (b) Bijel templated gas diffusion layer (GDL) in a PEMFC. Water is removed from the catalyst layer via the unaltered pores, whereas oxygen is supplied through the hydrophobized channels. (c) Covalently modified Janus nanoparticle with faces of opposite wettability. (d) Confocal micrographs of bijels fabricated via (i) thermal quenching,[10] (ii) STrIPS ,[15] (iii) coarsening of sheared emulsions,[21] (iv) small domain bijel structure produced by our research group, where a hydrophobic dye diffuses from the ambient oil into the oil channel.[17]

The intertwined pore systems of opposite wettability in functionalized bijels could serve as the gas diffusion layer in PEMFCs. Water would be drained via the unaltered, hydrophilic channel. Oxygen is not repelled by the coating and can diffuse through the hydrophobic pores. The asymmetric character transforms the bijel into a Janus porous material, which is named after the Roman god who had two distinct faces. Until now, such media were limited to bilayers.[22] A bijel would become the first material to extend the Janus character into three dimensions.

Recently, our group used STrIPS to drastically reduce the domain size in a scalable process (Figure 2d).[17] The Nobel laureate Wolfgang Pauli once issued a famous warning against the

fabrication of such materials: “God made the bulk; the surface was invented by the devil.” Nevertheless, the large interfacial area in bijels allows for intimate contact between the phases, which increases their potential as catalytic microreactors. Currently, only one chemical composition is known which forms *small-domain* bijels. A dried, phase-selectively hydrophobized bijel could serve as a template for other combinations of immiscible fluids. The introduction of a polar liquid, followed by an oil reconstitutes the same bijel structure, but with different phases (**Figure 3**). Hence, a Janus bijel greatly expands the solvent choice and increases the potential for bijel use in heterogeneous catalysis.

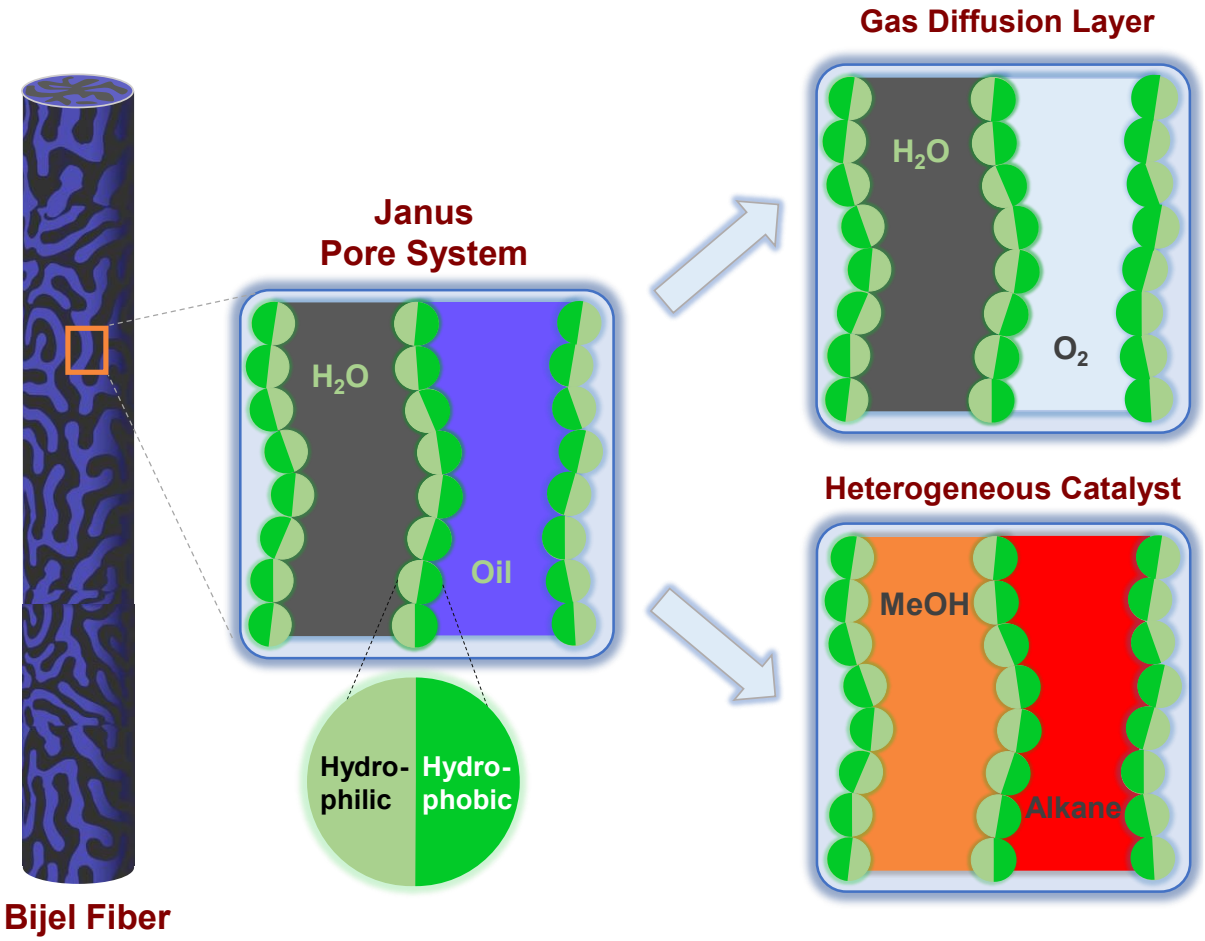

Figure 3: The Janus small-domain template could be filled with combinations of immiscible fluids. This structure could be used to regulate the pathways of water and oxygen mass transport in GDLs, or as a heterogeneous microreactor with intimate contact between solvents.

In this work, we focus on the following research questions:

1) How can we obtain a porous Janus material through phase-selective hydrophobization of the particle scaffold?
2) Will alkyltrichloro- or alkyltriethoxysilanes result in a more hydrophobic coating?
3) How can the surfactant be removed from the nanoparticle surface, and how does this change in wettability affect the bijel structure?
4) What is the role of the solvent during particle crosslinking?
5) How can we prevent the loss of phase distinction over time?

Section 4.1 deals with how we fabricate a small-domain bijel. This structure is used as a template for the porous Janus material. We deal with the influence of surfactant removal from the nanoparticles in chapter 4.2. How the temporal instability of the bijel structure hinders the fabrication of a Janus material, and our method to resolve these issues, is discussed in section 4.3. Finally, the phase-selective hydrophobization is discussed in chapter 4.4.

2. Literature Survey

Some background knowledge about particle-stabilized emulsions is necessary before we introduce how bijels could be used in the gas diffusion layer of PEMFCs. Once this understanding has been established, we will introduce the function of a GDL. Finally, we will outline the surface modification tools necessary to functionalize the bijel into a Janus porous material.

2.1. Particles at interfaces

Interfacial tension causes any system to minimize its surface area to lower its free energy.[23] Solid particles can aid in this process by assembling on the interface, which minimizes the contact between immiscible liquids.[24] In colloidal dispersions, these particles have a diameter between 1 nm and 1 µm.[25] Such particles can favor one phase over the other depending on their wettability. This preference is expressed in the so called *contact angle* θ, which is defined as the angle between the water-fluid and water-particle surfaces (**Figure 4**a).[26] The contact angle

changes depending on the wettability of the particle surface. The interfacial Gibbs free energy of a specific state (G) is given by

$$G = \gamma_{ow} A_{ow} + \gamma_{sw} A_{sw} + \gamma_{os} A_{os} \quad (2.1)$$

where γ is the interfacial tension and A the surface area of the oil-water, solid-water and oil-solid interfaces (*ow*, *sw* and *os*, respectively).

The gain in free energy of the attachment of a particle to the interface can be described as

$$\Delta G_{int} = -\pi r^2 \gamma_{ow} (1 - \cos \theta)^2 \quad (2.2)$$

with ΔG_{int} the change in interfacial Gibbs free energy, and r the particle radius.[27] Although this equation does not take into account line tensions, which contribute to the energy in nanoparticles, it is widely used to describe the adsorption to interfaces.[28] The free energy is at a minimum when the contact angle θ is 90° (Figure 4b). Nonetheless, any nonzero contact angle results in a decrease of the interfacial energy, although it should be significantly higher than the thermal energy for the particles to permanently adsorb to the interface. Because of the radius dependence of the attachment energy, small particles can only be used when the interfacial tension is sufficiently high.

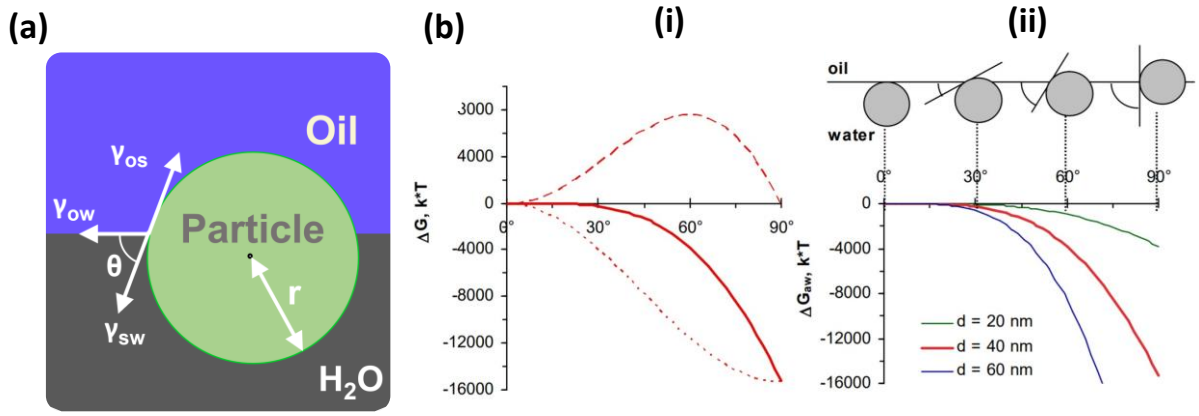

Figure 4: (a) Particle at an oil-water interface. θ is the angle between the particle and the aqueous phase; (b) interfacial attachment Gibbs free energy of spherical particles at the oil-water interface as a function of the contact angle; (i) dotted line: decrease of oil-water interface; dashed line: liquid-particle interaction; solid line: total of both contributions, (ii) for various particle diameters. For all graphs the interfacial tension γ_{ow} = 50 mN/m; Adapted with permission from ref. 27 (M.F. Haase, 2011).

2.2. Pickering emulsions

Particle attachment can stabilize fluid-fluid interfaces, as it reduces the contact between immiscible liquids. At sufficiently high concentrations, solid particles can lead to emulsification, as discovered by Walter Ramsden in 1904.[29–31]. These so-called *Pickering emulsions* are more stable against de-emulsification compared to traditional surfactant-stabilized emulsions.[32] Furthermore, the properties of the emulsion can be tuned directly via the pH, ionic screening and particle wettability.[33] The latter can be controlled via the electrostatic adsorption of an amphiphilic surfactant. Low surfactant concentrations result in a contact angle θ below 90° (**Figure 5**). Such particles impose an interfacial curvature away from the aqueous phase, which results in oil-in-water (O/W) emulsions. Analogously, further surfactant adsorption increases the contact angle above 90°, which leads to water-in-oil (W/O) emulsions.[34] In between these extremes the contact angle is exactly 90°, and particles become neutrally wetting. They allow curvature towards both phases, and are essential to the stabilization of the bicontinuous structure in bijels.[35]

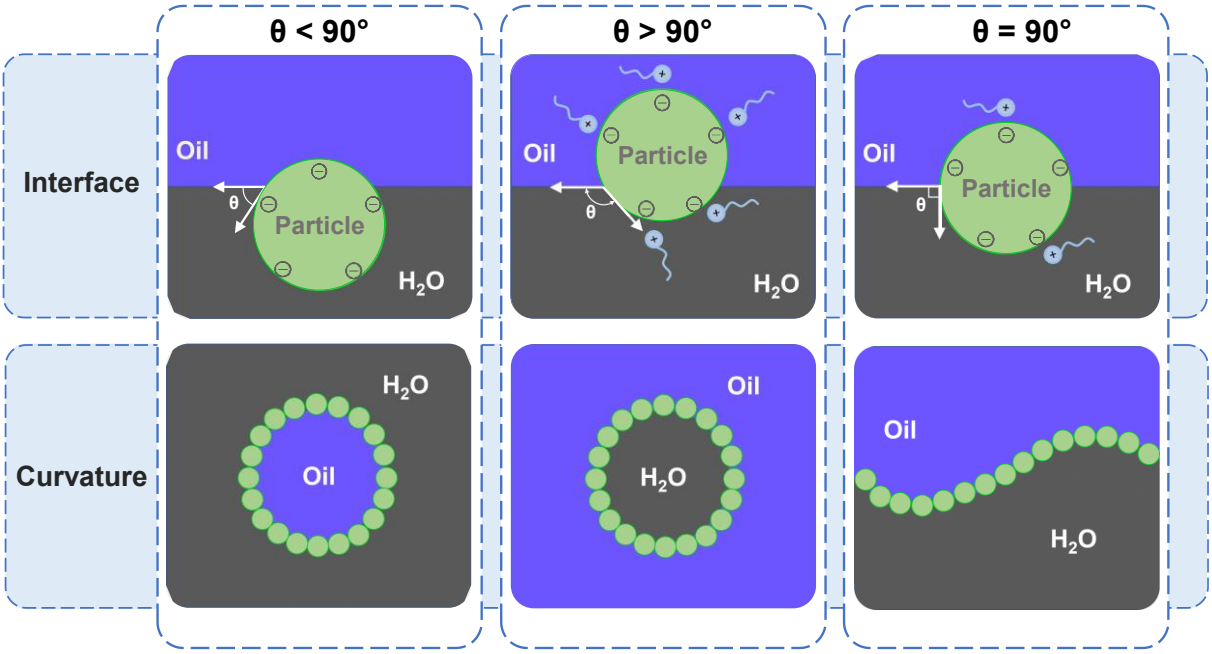

Figure 5: Solid particles at oil-water interfaces. Increased surfactant adsorption leads to more hydrophobic particles and a larger contact angle. O/W emulsions are stabilized at θ < 90°, whereas θ > 90° results in W/O emulsions. With neutrally wetting particles (θ = 90°) the surface can curve towards both constituents.

2.3. Bijels

As explained above, interfacially active particles can stabilize emulsions of immiscible fluids. These emulsions can be formed via e.g. the agitation of immiscible liquids,[36,37] but more commonly by phase-separation of initially homogeneous mixtures.[10] When a change in temperature or chemical composition puts the system below the so called *binodal coexistence curve*, the mixed state becomes metastable. Over time, phase-separation occurs via *nucleation and growth*. However, demixing occurs spontaneously in compositions below the *spinodal curve*, due to the absence of an initial thermodynamic barrier. Phase separation occurs throughout the system via *spinodal decomposition*, which proceeds via a bicontinuous arrangement.[38,39] The two coexistence curves meet in the *critical point*, where any phase boundaries disappear and there is no interfacial tension. The structures formed in both these separation routes are transient and coarsen over time to minimize the interfacial area.

However, the spinodal composition can be arrested by neutrally wetting particles. Interfacial jamming of the structure by these nanoparticles forms a *bicontinuous interfacially-jammed emulsion gel* (**bijel**). Such a material consists of two interwoven, fully continuous channel networks with a large surface area. This unique type of Pickering emulsion was initially predicted by computer simulations in 2005,[40] and first fabricated in the lab two years later.[10] Since then, bijels have been used as templates for porous materials,[41–43] electrodes,[11,44] aerogels,[45] microcatalysts[19,46] and in edible products.[47]

2.4. STrIPS

Bijels are commonly made in batch processes such as thermal quenching.[48] A rapid change in temperature leads to spinodal decomposition of initially miscible liquids. The few pairs of liquids which can be used, do not have a large interfacial tension in the demixed state. Therefore, only large particles can arrest the bicontinuous structure (formula 2.2). This issue was resolved in 2015 with the introduction of *Solvent Transfer-Induced Phase Separation* (STrIPS).[15] With this method, bijels can be fabricated with pairs of liquids with high interfacial tensions, which facilitates the use of nanoparticles. The presence of a co-solvent allows for an initially homogeneous mixture with oil and water at room temperature. The subsequent removal of solvent triggers spinodal decomposition, because the initial composition is near the critical point (**Figure 6**a). Meanwhile, the removal of solvent makes the liquid more apolar. The solubility of the surfactant *cetrimonium bromide* (**CTAB**) decreases, since the increasingly

more apolar liquid can no longer stabilize the charged groups in the surfactants. [49,50] The subsequent electrostatic adsorption of CTAB to the charged Ludox TMA surface leads to *in-situ* modification of the nanoparticles.[16] The bicontinuous arrangement is arrested when i) the interfacial tension is high enough to facilitate interfacial jamming and ii) the nanoparticles have become neutrally wetting (Figure 6b). Importantly, STrIPS can be used to scale up bijel production as it allows for the continuous production of fibers with the aid of microfluidics (Figure 6c, section 2.5).

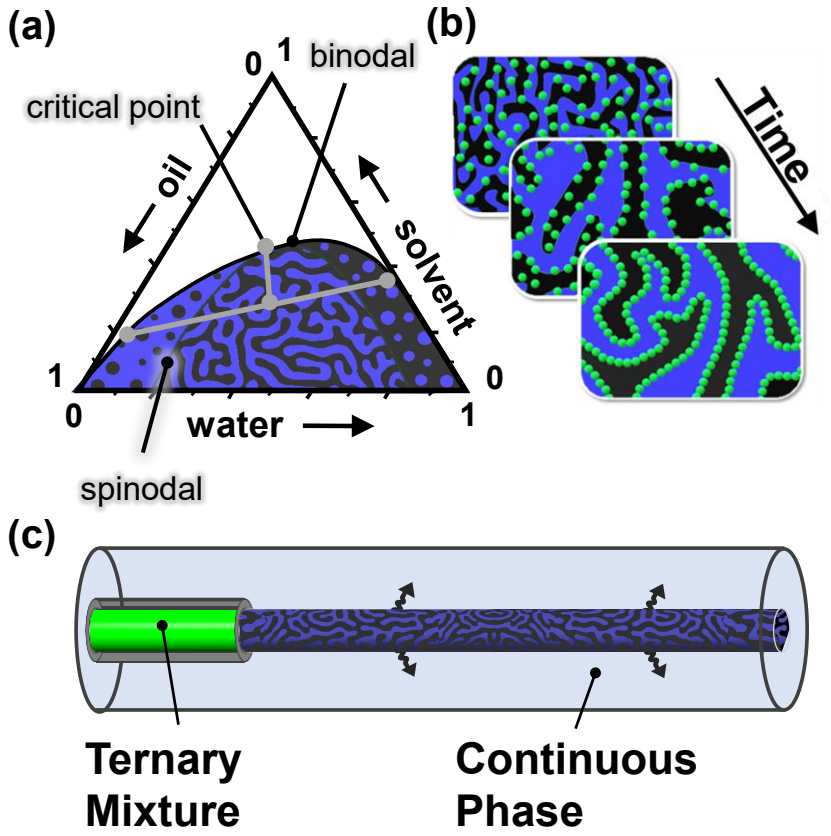

Figure 6: STrIPS bijel formation, (a) solvent depletion from a ternary mixture induces spinodal decomposition, which results in the compositions on either side of the tie line, (b) nanoparticles jam onto the interface of the forming bijel, (c) solvent diffusion from a ternary mixture into a continuous phase. Adapted with permission from ref. 51. Copyright American Chemical Society (2019).

2.5. Microfluidics

In contrast to conventional processes, STrIPS facilitates the continuous fabrication of bijel fibers because of the use of microfluidics. A ternary mixture is injected into a continuous phase

(Figure 6), which takes up the solvent and induces spinodal decomposition. The flow in such devices can be described with quantities from fluid dynamics, such as the *Reynolds number* (Re),

$$Re = \frac{v\,L\,\rho}{\mu} \tag{2.3}$$

where v is the characteristic velocity, L the characteristic length, ρ the density and μ the dynamic viscocity.[52] Similarly, the *Peclet number* (Pe) gives the ratio between convective and diffusive transport,

$$Pe = \frac{v\,L}{D} \tag{2.4}$$

with D the mass diffusion constant.[53] The small size of a microfluidic apparatus results in small Re and Pe numbers, and hence the flow is nearly always laminar.[54] Therefore, diffusion dominates transport by convection, which allows for great control over the extrusion parameters in STrIPS. The short diffusion length allows for rapid removal of the solvent from the ternary mixture, which ensures the phase separation is halted at an early stage of coarsening.

2.6. Small domain bijels

The pores in bijels have gotten increasingly narrow since the production of the first bijel (Figure 2d). However, until recently sub-micron channels could only be achieved in batch processes.[21] STrIPS was introduced in 2015, which allows for the continuous production of bijel fibers. A solvent is extracted readily from the ternary mixture when it favors partitioning towards the continuous phase. Recently, M.A. Khan and A.J. Sprockel et al. found that 1-propanol diffuses rapidly from a ternary mixture with diethyl phthalate (DEP) and water.[17] The adsorption of surfactant leads to *in-situ* modification of the particle surface. This effect works synergistically with rapid solvent transfer, which leads to a sharp increase in interfacial tension. Therefore, spinodal decomposition can be arrested at an early stage of coarsening. Secondly, due to the large interfacial tension, nanoparticles can be used (formula 2.2). Nanoparticles can stabilize the large interfacial area because of their large surface-area-to-volume ratio.

This novel fabrication method results in domains between 500 nm and 2 μm in diameter, and a bijel surface-area-to-volume ratio of 2 m^2/cm^3. The mass transport of lipophilic dyes from the ambient oil shows that chemicals can radially diffuse into the oil phase. Conversely, the water channel is isolated from the surroundings by the particle scaffold, and the axial dimension of

the fibers is too large to facilitate diffusive transport. Instead, electro-osmosis allows for transfer of chemicals throughout the aqueous phase. So far, the aqueous phase has not been exchanged for other polar media.

2.7. Confocal microscopy

Bijels are commonly visualized and characterized with confocal fluorescence microscopy.[10,15,21,55] Contrary to brightfield methods, these microscopes record the fluorescent response upon irradiation of a sample with a specific wavelength.[56] The wavelength of the emitted fluorescent light changes depending on the solvent, a principle called *solvatochromism*.[57] Dyes can therefore be used to visualize the phase distinction in bijels (**Figure 7**). In regular microscopes, the signal is obscured by that from neighboring, out-of-focus planes. Confocal microscopy resolves this issue, as it uses a pinhole which only lets light from a single focal plane through.[58] This point-scanning technique allows one to image an object one slice at a time, which can be combined into so called *z-stacks* to obtain 3D reconstructions.[59]

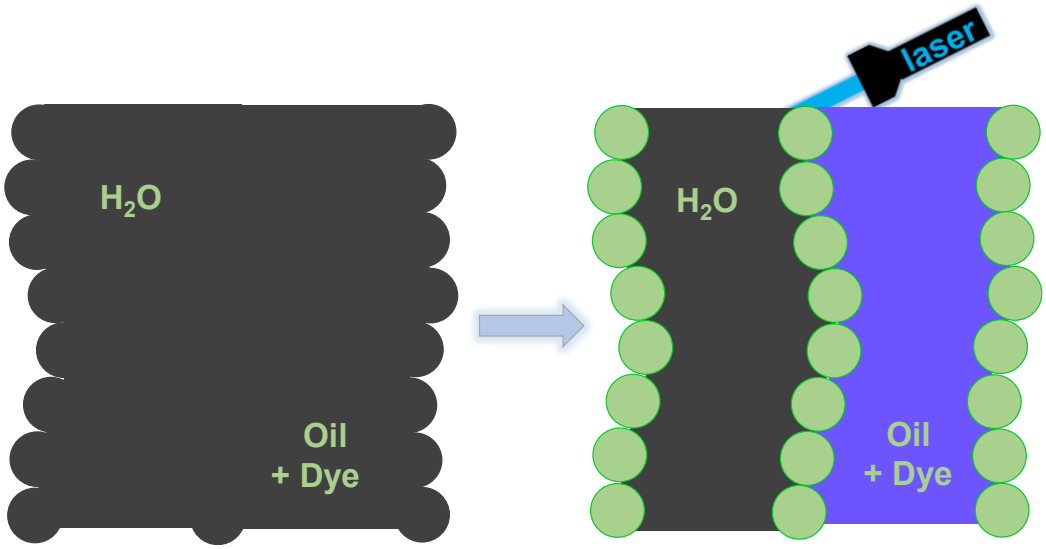

Figure 7: Upon illumination with a laser, fluorescence is only observed in regions where the dye is present. The wavelength of fluorescence varies depending on the chemical environment of the dye (false colors are used).

2.8. Surface modification

STrIPS uses Ludox TMA particles, which consist of silica with alumina inclusions. The colloidal properties can be expanded from that of the bulk material through modification of the

particle surface. For instance, ligands can be placed on solid particles through chemisorption, the hydrophobic effect, or the electrostatic adsorption of amphiphiles.[60] In TMA, the superficial hydroxyl groups also allow for covalent modification with the use of chloro- and alkoxysilanes.[61,62] These substituents are hydrolyzed, after which the unit undergoes a condensation reaction with the superficial hydroxyl groups. The pH, ionic strength and temperature influence the reaction kinetics.[63,64] Chlorosilanes react more readily than alkoxysilanes. The hydrolysis rate is inversely related to the length of the alkoxy chain due to increased steric hindrance. The multiplicity of the formed layer can be tuned with the number of hydrolyzable substituents. A single hydrolyzable substituent leads to the formation of a monolayer, whereas a network forms when the number of these groups are increased.[18]

2.9. Crosslinkage of nanoparticles

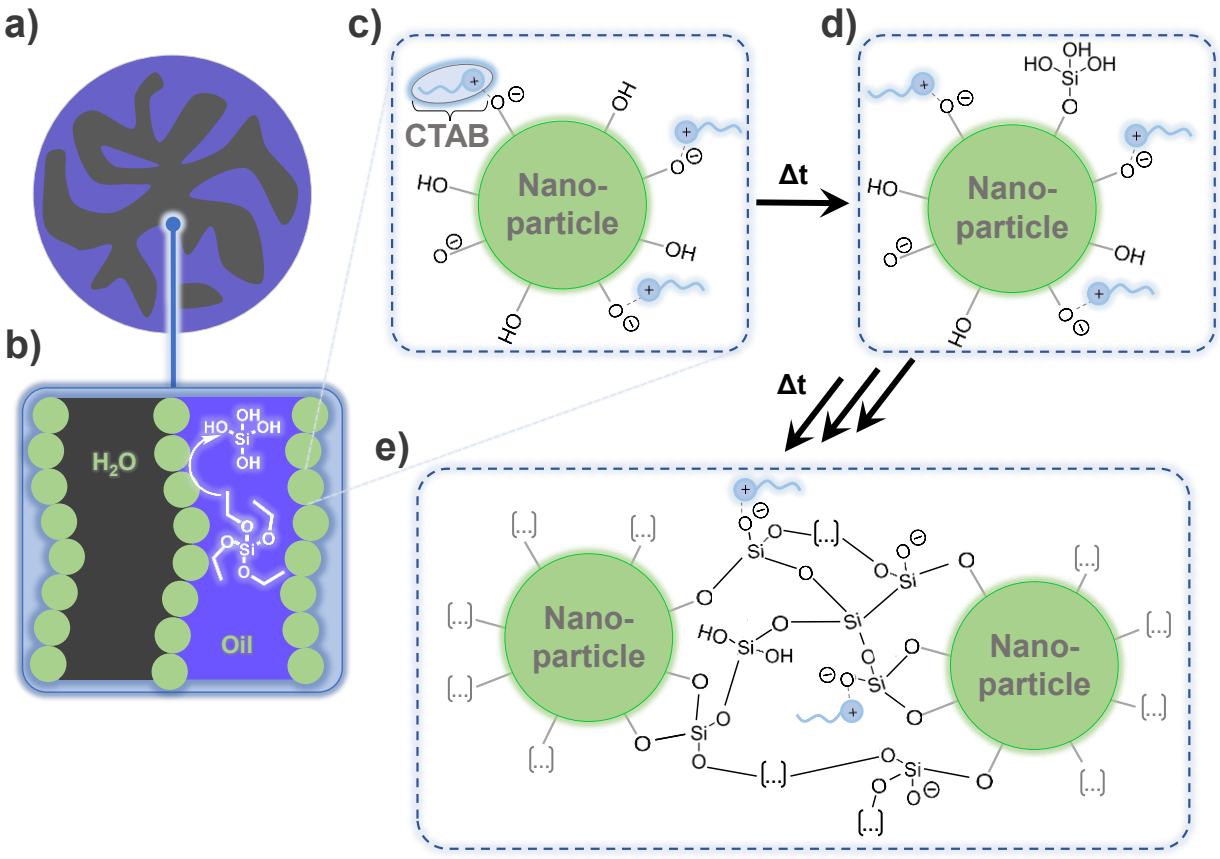

Figure 8: Crosslinking of nanoparticles, (a) cross section of a bijel fiber, (b) TEOS hydrolysis at the oil-water interface, (c) nanoparticle in a fresh fiber, (d) hydrolyzed TEOS has condensed onto the surface, (e) an interconnecting network forms over time.

One silane which has been used in bijels is t*etraethylortho silicate* (**TEOS**). This tetraethoxysilane is used for the fortification of the interfacial scaffold, such that bijels are robust against changes in interfacial tension, pH or ionic screening. Without the reinforcement, changes in these parameters would make particles lose their interfacial activity.[19] TEOS can be added to the ternary mixture in STrIPS, after which it partitions to the oil phase and is hydrolyzed at the oil-water interface. Subsequent condensation with the surface hydroxyl groups deposits extra silica (**Figure 8**).[65,66] This process crosslinks the nanoparticles, which results in a more durable and mechanically resilient material. Dried TEOS-treated bijels can withstand the capillary stresses of solvent evaporation. Afterwards, bijels can be visualized using *scanning electron microscopy* (SEM).

2.10. Hydrogen fuel cells

Bijels consist of an aqueous phase and a hydrophobic oil, and hence are materials with patterned wettability. This category of materials is also used to increase the efficiency of hydrogen fuel cells. The generation of electricity with such devices is a promising tool in the transition to fully sustainable energy. Problematically, the intermittency of renewable energy led to fluctuations in the amount of generated energy, and the demand for electricity would not always be matched. To resolve this issue, green electricity can be used to hydrolyze water to hydrogen gas at moments of excess production (Figure 1). When green energy production falls short, hydrogen fuel cells allow for the harnessing of electricity via the opposite reaction. Importantly, the oxidation of hydrogen forms only water and does not release carbon into the atmosphere.[3,4]

A *proton-exchange membrane fuel cell* (**PEMFC**) is commonly used for this process.[5] At the anode, hydrogen is split into protons and electrons. Because the anionic polymer membrane is only permeable to protons, the electrons are forced through an electrical circuit, and electricity is generated. These two species combine with oxygen at the cathode to form water. The *gas diffusion layer* (**GDL**) regulates the removal of the product. Problematically, most GDLs do not contain separated pathways for water and oxygen transport. The lack of regulation increases the diffusion length of oxygen transport and decreases the fuel cell efficiency. State-of-the-art GDLs contain regions of opposite wettability, which form separate channels for the mass transfer of oxygen and water in opposite directions. These methods raise the power output of PEMFCs, since the oxygen reactant is supplied to the electrode more readily. Importantly, simulations have shown that broad pores will fill with water independently of their wettability.[9]

Therefore, a porous material with narrow channels of opposite wettability should increase the power output of hydrogen fuel cells.

2.11. Janus porous materials

A medium with one hydrophobic and another hydrophilic pore system would meet the requirements for a GDL with patterned wettability. The porous character means it has a large surface-area-to-volume ratio, which lends such materials for applications in catalysis,[67] insulation materials[68] and as electrodes.[69,70] The opposite wettability within the same system makes it a *Janus porous material*, named after the Roman god who had two unique faces.[71–74] A Janus material contains asymmetries in e.g. charge, chemical composition, reactivity, or conductivity.[75] Janus porous materials combine both these characteristics and are already used to regulate gas and liquid transport.[76–83] Currently, most asymmetric porous media consist of bilayered structures, as it remains difficult to extend the Janus character to 3 dimensions.[22]

3. Materials and Methods

All solvents used for the experiments were HPLC grade. Toluene (>99.85%), n-Hexane (>99% HPLC), both acquired from Acros Organics, and mineral oil and 1-octanol (>99%), both obtained from Sigma-Aldrich were water saturated. Dodecane (mixture of isomers), glycerol (>99%) and diethyl phthalate (DEP, 99%) were purchased from Acros Organics and used without any further purification. 1-propanol (99.5%), hexadecyl-trimethylammonium bromide (CTAB, >99%), Nile red, tetraethyl orthosilicate (TEOS, >99%), LUDOX ® TMA and NaCl were acquired from Sigma-Aldrich UK and used without additional purification. Water was purified with a MiliQ Synergy system before use, with a conductivity below 18.2 MΩ cm^{-1}.
n-octadecyltrichlorosilane (OTS) and n-hexyltriethoxysilane (HTES) were purchased from Santa Cruz Biotechnology and were stored under inert atmosphere. Epoxy adhesive from LIQUI MOLY and 1 mm diameter needles from Weller were acquired. Round capillaries of inner diameter (ID) of 50 µm and 300 µm and square capillaries of inner-cross sections of 100 µm and 900 µm from VitroCom were scored and broken to the desired size using ceramic tiles from Sutter Instruments. Cole parmer AWG thin wall tubing of 0.9 mm ID from Cole-Parmer of microfluidic device was connected to syringes at Aladdin SyringeONE pumps by World

Precision Instruments. Spectral/Por® molecular porous membrane tubing from Spectrum was used for particle dialysis.

3.1. Aqueous phase

LUDOX ® TMA was concentrated from 34 to 45 wt.%. Initially a hot plate (70 °C, 2 h) was used, but later we switched to rotary evaporation (142 mbar, 60 °C, 20 min). Particle aggregates were removed via centrifugation (3273 g, 10 min, 50 mL/26 mm ID tube). Thereafter, 1 M HCl (aq) was added to reach pH 2.9. The salt concentration was equilibrated through dialysis with a reservoir containing 4 L of 50 mM NaCl (aq). Multiple pH and salt concentrations were used in parametric optimization, but the optimum was generally pH 2.9 and 50 mM NaCl. The nanoparticles were diluted to reach a final concentration of 40 wt.% in the *aqueous phase*.

3.2. Solvent phase

CTAB was added to 1-propanol to prepare a 200 mM CTAB in 1-propanol stock solution. The mixture was sonicated to break up the solid. To dissolve the surfactant the temperature was increased with 5, 3-second heating intervals on a hotplate (80 °C), followed by vortex mixing. Care was taken to prevent solvent evaporation. Subsequently, 50 wt.% glycerol in 1-propanol was added, which was necessary for refractive index (RI) matching. Finally, 1-propanol was added to attain a final concentration of 30 wt.% glycerol in the *solvent phase*. The optimal surfactant concentration was varied per experiment and was found by quick fiber extrusions of ternary mixtures which contained between 50 and 70 mM CTAB in the *solvent phase*.

3.3. Ternary mixtures

A ternary mixture of water, oil and solvent was prepared with a composition close to the critical point ($\varphi_{wat} = 0.50$, $\varphi_{oil} = 0.070$ and $\varphi_{solv} = 0.43$). The *oil phase*, which consisted of diethyl phthalate (DEP) was combined with the *solvent phase* and the *aqueous phase*. The volume fractions of the pure liquids, without taking the particle volume into account, are shown **Figure 9**.

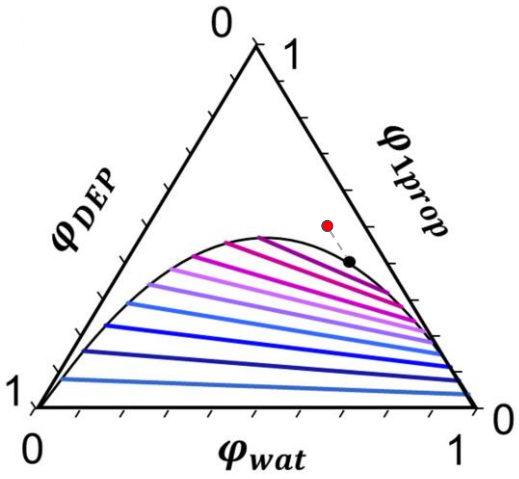

Figure 9: Ternary phase diagram of pure DEP, 1-propanol and water, with critical point (black dot). The red spot indicates the volume fractions of the ternary mixture when only the *pure constituents* are considered in (φ_{wat} = *0.42*, φ_{oil} = *0.08* and φ_{solv} = *0.50*). Adapted with permission from ref. 17. Copyright John Wiley & Sons (2022).

3.4. Microfluidics

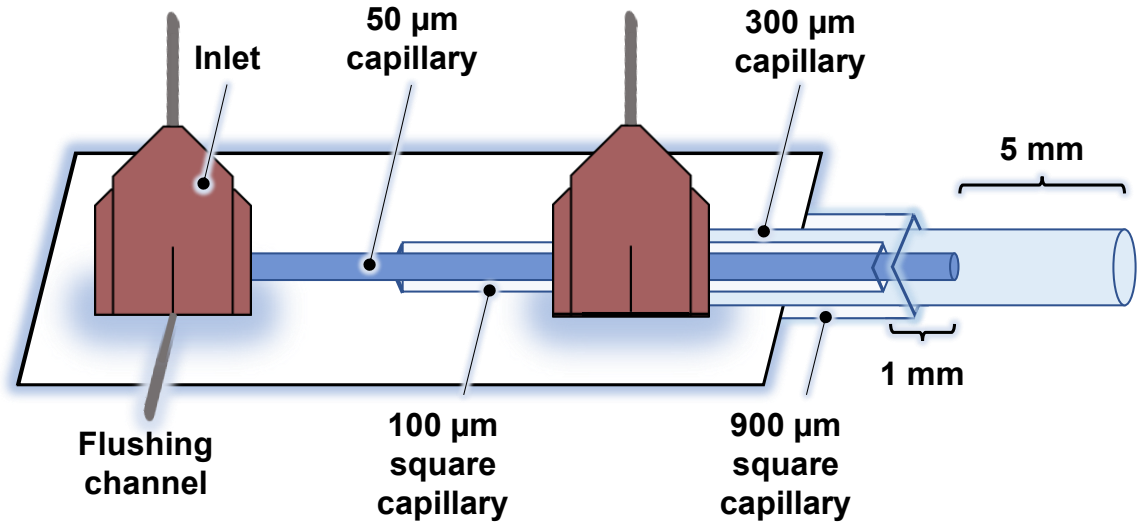

Figure 10: Microfluidic device used to extrude bijel fibers.

50 µm and 300 µm inner diameter (ID) capillaries were scored with a ceramic tile and broken carefully to create a smooth orifice. The latter was fixed on a microscopy slide using epoxy resin. UV glue was used to fix the small capillary inside a square 100 µm ID capillary, which helped to place the 50 µm capillary exactly at the center of the 300 µm one. Epoxy resin was applied to the 100 µm capillary to attach it to the microscopy slide. Because the nozzle broke frequently, an outer 900 µm square capillary was added for support. The end was closed with

epoxy. For the inlets, the bottom of the plastic needles was cut and small insertions were made with a razor blade to create openings for the capillaries and flushing channel. 2-3 drops of epoxy were used to fix the needles to the microscopy slide. Viscous, almost cured epoxy was used to seal the openings, after which a copious amount of glue was applied to reinforce the device. After 4 hours the epoxy had cured and the device was filled with OTS and left for 18 hours to hydrophobize the nozzles.

3.5. Extrusion and printing

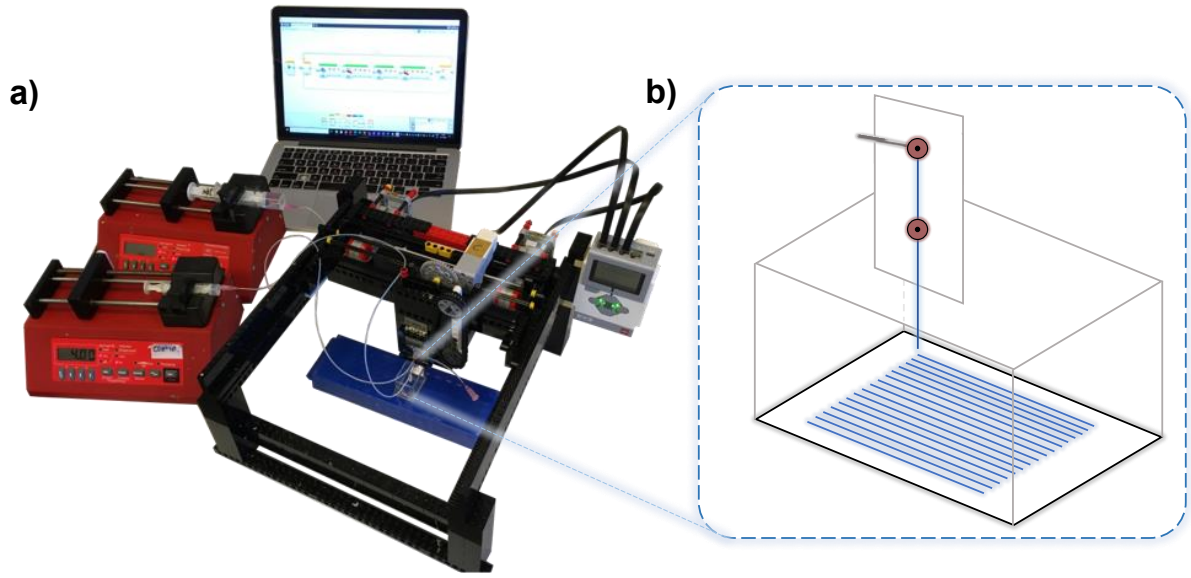

Figure 11: Extrusion setup, (a) syringe pumps and LEGO printer with associated Mindstorms software. Adapted with permission from ref. 17. Copyright John Wiley & Sons (2022), (b) fiber extrusion from the microfluidic device.

The centering of the capillaries was analyzed with a brightfield microscope. Syringes containing 2-3 mL ternary mixture and another with 20 mL toluene were placed in the pressure pumps after the removal of any air bubbles. The ternary mixture was attached to the inlet with the flushing channel via tubing, toluene to the other needle (**Figure 11**). The channels were flushed with their respective fluids. Toluene was flown at 1 mL/min through the 300 µm capillary until all bubbles had left the tubing, and the rate was changed to 15 mL/h. Afterwards the ternary was flown out of the flushing channel at 1 mL/min. The flushing channel was closed off with an epoxy-filled needle and the 50 µm capillary was flushed for 5 s until it was completely filled with liquid. LEGO® Mindstorms® was used to move the device nozzle at a tunable speed in a bath of 7 mL toluene. The flow rate of the ternary mixture was set to 0.5

mL/h. The flow rate of toluene and the printer speed were tuned such that continuous, dilation-free fibers were extruded (section 4.3.3), generally around 10 mL/h and 22-24 LEGO units (L.U.), respectively. The submerged nozzle was placed at a height of 1-2 cm to facilitate the diffusion of 1-propanol from the fiber. 2 rounds of 60 fibers each were printed continuously, which took 2 minutes to complete. A brief purge of toluene usually unclogged the device, otherwise the same procedure was used for both liquids. When this did not help the device was flushed with ethanol under sonication.

3.6. Quick fiber extrusion

For parametric optimizations of the bijel structure continuous fibers were unnecessary and a faster method of extrusion was used. A 50 µm ID capillary was fixed in a pipette tip using UV-curable adhesive. The nozzle extended 2-3 mm from the pipette tip. The other end of the capillary inside the pipette tip was broken at the cured glue. 20 µL of ternary mixture was extruded in a container of toluene at a height of 1-2 cm to allow for proper diffusion of 1-propanol while the fiber sank to the bottom.

3.7. Washing procedure

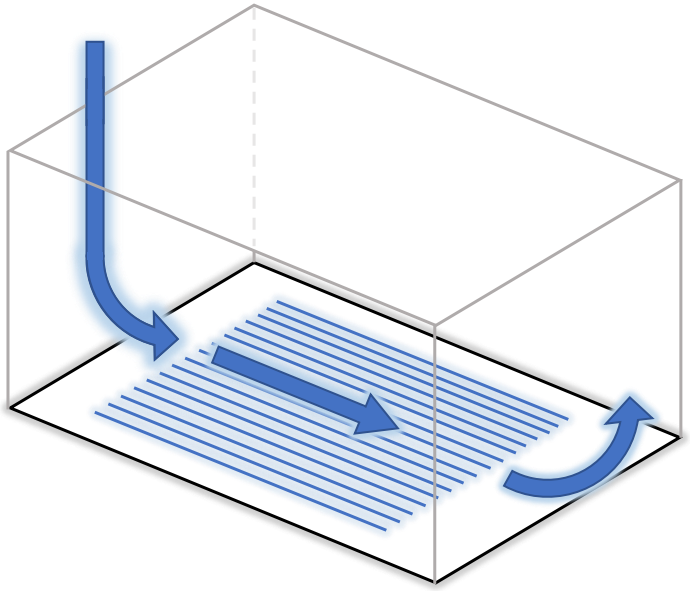

Figure 12: Liquid flow over the fibers during washing.

The ambient liquid was removed, taking care that the fibers were still covered to prevent capillary stresses due to evaporation. In non-volatile liquids such as dodecane and mineral oil these effects were not a concern. 2 mL of fresh liquid was gently flown via the corner of the container to minimize shear stress and removed from the opposite side. The same liquid was flown over the fibers 4-5 times to ensure proper mixing (**Figure 12**). The procedure was repeated with fresh liquid, which was replaced with 2 mL of liquid. The number of *washing steps* signifies the total introductions of fresh liquid. When non-viscous fluids such as toluene, hexane and dodecane were replaced with viscous mineral oil, the container was tilted to dampen the impact of the injected liquid. The incline was not necessary with mineral oil as ambient phase because of its high viscosity.

3.8. Confocal microscopy

The Leica Stellaris 5 confocal microscope was used with Nile red in hexane as fluorescent dye. A 488 nm laser induced fluorescence in the oil channel, which was recorded at 500-550 nm. A 561 nm laser was used to monitor the nanoparticles between 600 and 700 nm to prevent spectral overlap with the oil (appendix 1). During imaging, the laser intensity was used to tune fluorescence, and the gain was kept at a minimum. For spectral scans a region of interest (ROI) was used to only monitor the fluorescence inside the fiber (appendix 2).

3.9. Scanning electron microscopy (SEM)

Fibers were washed with hexane and 1-propanol and dried overnight to remove the phase constituents. Rectangular LEGO pieces were cut to fit onto an SEM stub and covered with carbon tape. The LEGO piece was gently covered with fibers which were subsequently sputter coated with a 9 nm layer of platinum. Phenom ProX was used to record the micrographs.

3.10. Image processing

The raw confocal micrographs were processed in ImageJ. The minimum and maximum intensity were changed such that the background was of homogeneous intensity. One was the signal from the fiber, the other the background. If necessary, the contrast was adjusted more (appendix 3). An overlay of the two channels was created and a scalebar was inserted for reference. For the spectral scans, the fluorescence was recorded in a range of 460-800 nm, at intervals of 3.01 nm. The fluorescent response was measured at a specific wavelength $\pm$ 15 nm.

3.11. TEOS-treatment

Freshly printed fibers were washed with a solution of 3 wt.% tetraethyl orthosilicate (TEOS) in water saturated mineral oil as described in section 3.7. After 18 hours the mixture was replaced with fresh mineral oil.

3.12. Octanol wash

TEOS treated fibers were washed with water saturated octanol. After 1-3 washing steps, octanol was replaced by mineral oil. A fourth, additional washing step was included to ensure complete removal of the viscous octanol. Spectral scans were recorded as described in section 3.8.

3.13. Phase-selective hydrophobization

1 wt.% and 5 wt.% solutions of HTES and OTS in mineral oil were prepared. Week-old batches of TEOS-treated fibers, one washed with octanol, the other unaltered, were used per solution. The ends were cut with a razor blade and were covered with a water droplet to prevent exposure of the water phase to oil. The bottom of the containers consisted of a hydrophilic microscopy slide. When hydrophobic glass slides were used, the fibers wetted completely due to the favorability of the fiber-water interface over the glass-water interface. Initially, a water droplet was placed on the fiber endings to prevent contact between the aqueous bijel phase with the reagent. Unfortunately, the octanol washed fibers were wetted entirely by the droplet for the 1% HTES experiments. Therefore, all other octanol-washed batches were treated without the water droplet. After 18 hours the fibers were washed with mineral oil to remove the reagent. The fibers were washed with hexane and 1-propanol, and dried overnight to remove the phase constituents. Water droplets were placed on the fiber endings to refill the unmodified pore system. After 2 hours, hexane with Nile red was added and confocal microscopy was used to characterize the reconstitution. Reference micrographs of (un)hydrophobized fibers were recorded by rewetting with only Nile red in hexane or rhodamine-B in water.

4. Results and discussion

4.1. Structural optimization: parametric variation of pH, salt and surfactant concentration

STrIPS allows for the continuous fabrication of bijels through the rapid removal of solvent from a ternary mixture. We chose the starting composition to be close to the critical point, such that phase separation occurs via spinodal decomposition (Figure 9). The bicontinuous structure is arrested through interfacial jamming of neutrally wetting nanoparticles.[15,17] Together with M.A. Khan, the bijel structure was optimized for a) bicontinuous domains, b) a small radial pore size gradient, c) the absence of oil droplets, d) minimal particle aggregation, e) few *radial channels*. More specifically, a bicontinuous structure should consist of two fully continuous, uninterrupted networks on either side of the particle scaffold. The optimized structure is shown in **Figure 13**.

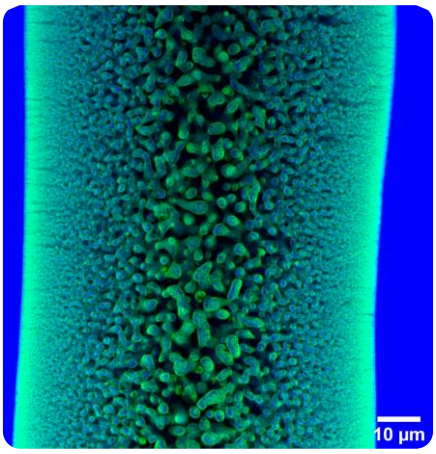

Figure 13: Freshly printed bijel fiber of the optimized composition (pH 2.9, 50 mM NaCl and 60 mM CTAB). The oil phase is shown in blue, the particles in green and the water in black (false colors).

Many parametric optimizations of the bijel structure were performed over the course of this research project. One such study is shown below (**Figure 14**). We varied the particle wettability through (i) **the amount of** amphiphilic **CTAB**, (ii) the surface charge via **the pH**, [84] and (iii) the charge-screening via the **ionic strength**.[85] Only certain combinations of parameters resulted in a bicontinuous arrangement. In some structures, the emulsion consisted of isolated sections, since the dye could not diffuse into the interior. Other combinations of the parameters did result in bicontinuous domains, but the criteria (b)-(d) were non-optimal. When particles are not neu-

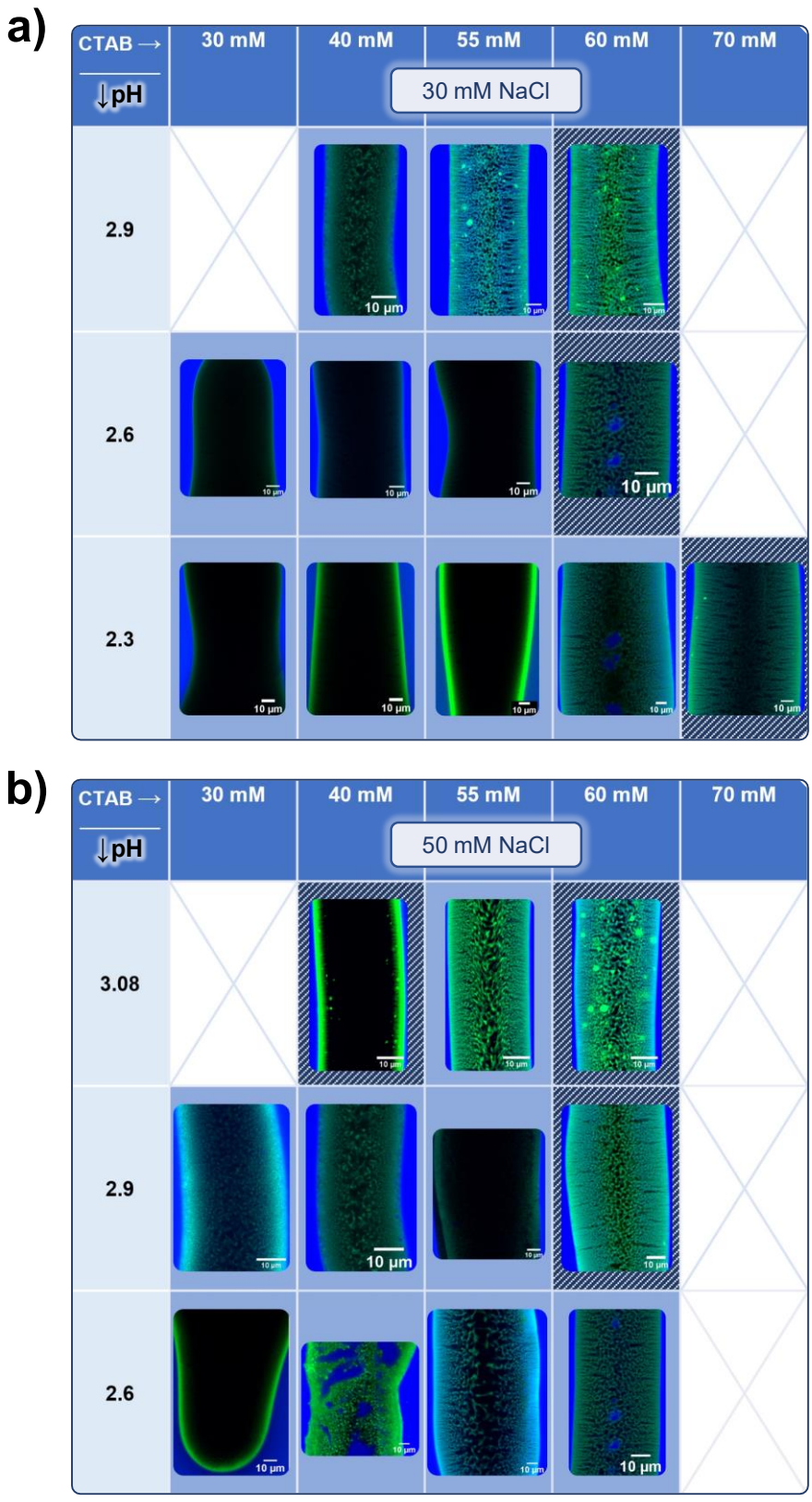

Figure 14: Parameter study to optimize the bijel structure for different pH and CTAB concentrations, (a) 30 mM NaCl, (b) 50 mM NaCl. The shaded cells represent ternaries that had gone slightly turbid. Crossed cells mark ternaries where the nanoparticles could not be dispersed at all.

trally wetting, they impose a curvature of the interface which leads to droplet formation. (b) and (c) disappeared with higher CTAB, but (d) and (e) became more prevalent.

(i): At low CTAB concentrations the particles maintained a significant surface charge. Possibly, the system was driven towards phase separation to promote stabilization of the highly charged particle surface in the aqueous phase. Conversely, excessive CTAB promoted particle flocculation in the ternary mixture due to the hydrophobic effect. Furthermore, the adsorption of the oppositely charged surfactant also lowered the zeta potential of the TMA surface, which decreases inter-particle repulsions. Bijels could be fabricated when CTAB was slightly above the optimum concentration, but the particles would aggregate inside the oil channel.[16] Finally, we found high CTAB increases the number of radially aligned channels. We do not currently have an explanation for these wide pores, although we suspect they could be caused by a Marangoni flow, driven by surface tension gradients. (ii) At lower pH, more CTAB was needed to obtain optimal structures. We propose that at low pH, the smaller charge density on the particle surface decreases the electrostatic attraction between the surface and the cationic surfactant. To balance this lower driving force, a higher CTAB concentration is needed to achieve the same surfactant adsorption. (iii) Ionic strength. The particle aggregation was slightly more pronounced at high salt concentration, which can be explained by stronger charge screening and decreased particle-particle repulsions. Additionally, positively charged species such as CTAB have been shown to adsorb more strongly at higher ionic strength.[86] At constant pH and high salt concentration, a lower CTAB concentration already resulted in bicontinuous domains. Due to increased screening, the zeta potential was not as far reaching, and less CTAB was needed to compensate the surface charge.

Generally, the parameters (a)-(e) were optimal at an ionic strength of 50 mM NaCl and pH 2.9 $\pm$ 0.03. The optimal CTAB concentration varied per batch of particles. Before each experiment, we varied the surfactant concentration at the aforementioned pH and ionic strength. In most experiments the optimum CTAB concentration was between 55 and 65 mM. Importantly, we found that the pH of the nanoparticle dispersion increased over time. We attribute this to two origins: (1) the protons take longer than one night to diffuse through the Stern layer, and the pH of the surface had not yet equilibrated with that of the liquid. (2) The alumina : silica ratio in the surface of TMA particles varies, since it is unclear if this ratio is constant per production batch. Additionally, silica tends to dissolve over time, which would increase the relative amount

of alumina.[87,88] A more clear understanding of these phenomena could eliminate the cumbersome CTAB optimization at the start of each experiment.

4.2. Surfactant removal

4.2.1. Initial hydrophobization findings

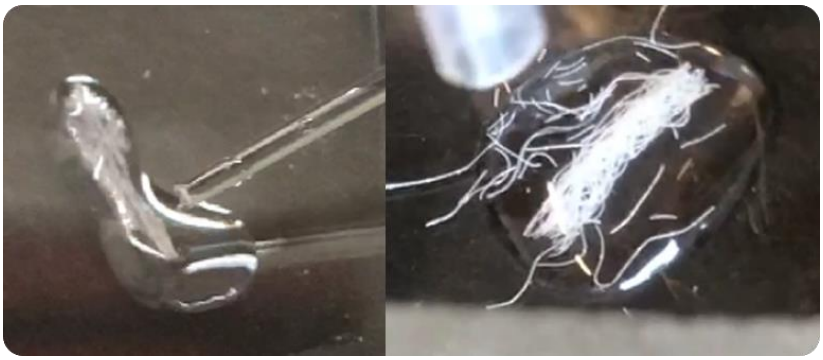

Figure 15: Water droplets were introduced to HTES-treated fibers to probe their wettability. Contrary to expectation, the droplet completely covered the fiber, which indicated a hydrophilic character.

The ultimate goal of this work was to fabricate Janus bijels. We hypothesized that one pore system could selectively be hydrophobized, whereas the other would remain hydrophilic. The migration of oleophilic dyes from the ambient phase into the bijel in confocal microscopy showed that chemicals can diffuse into the oil phase. Therefore, we expected that reagents such as silanes could also be transferred into the oil channel. Initially, we used the oil soluble *n-hexyltriethoxy silane* (**HTES**) in dodecane (1 wt.%, 18 hours). The fibers were dried post-treatment, after which only the scaffold remained. We expected the surface to be hydrophobized, since the fibers were submerged in oil during the treatment and the exterior was exposed to the reagent. To test the hydrophobicity, a water droplet was introduced to the surface. Unexpectedly, the fiber wetted readily as it was brought into contact with the water droplet (**Figure 15**). We hypothesized that CTAB impeded the reaction, since it binds to the same hydroxyl groups where HTES should react. Additionally, CTAB forms micelles which retard the formation of a polymeric silica network in the liquid.[89] Consequently, we investigated the influence of the removal of CTAB on the hydrophobization treatment.

4.2.2. Octanol wash

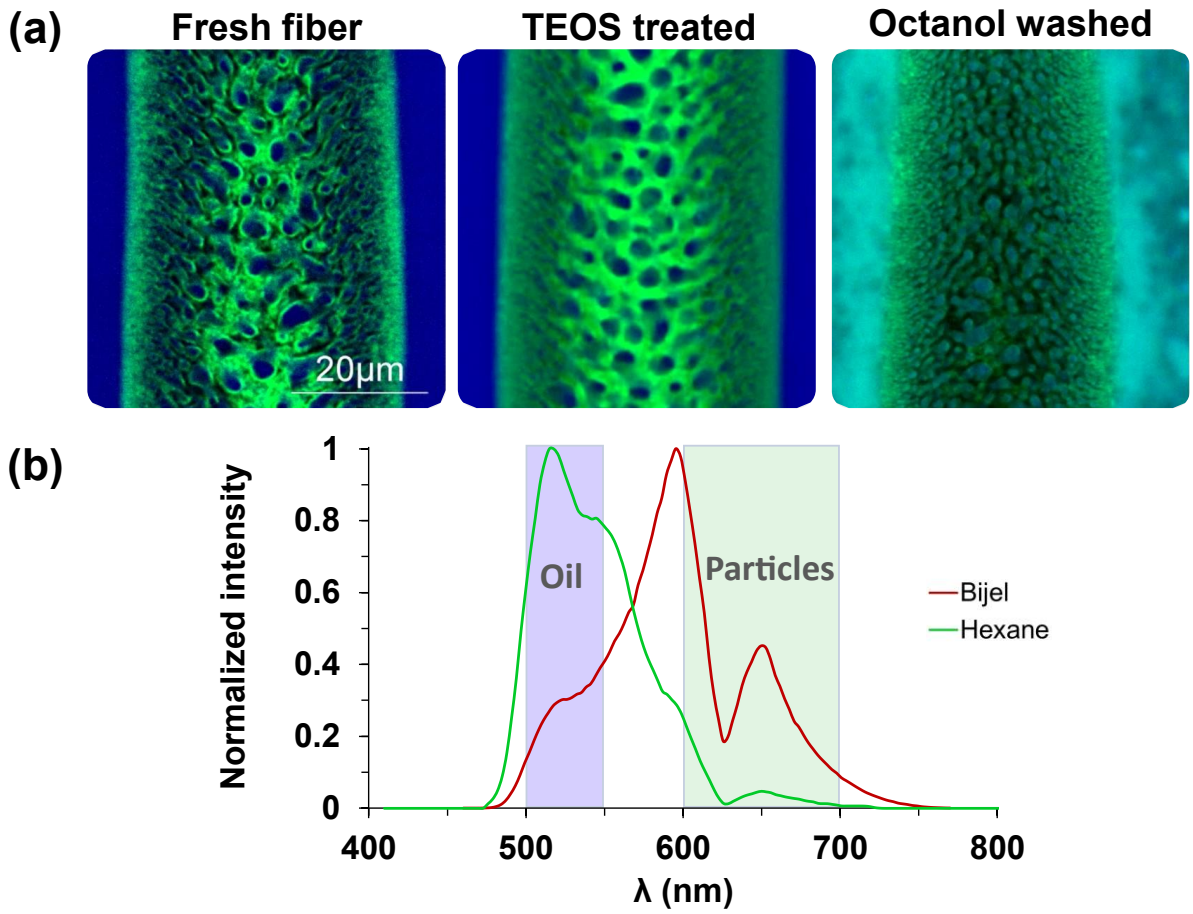

Figure 16: (a) Confocal micrographs of bijels extruded from a ternary mixture of 2-propanol, DEP and water. The additional silica surface after TEOS-treatment increases the signal intensity. Washing with octanol removes CTAB and thereby decreases the fluorescence intensity of the particle channel in large domain bijels (M.F. Haase). (b) Nile red fluorescence in hexane and inside a bijel. The oil-channel fluorescence was recorded in wavelengths 500 - 550 nm, and the particle channel between 600 - 700 nm. Each λ-scan was normalized individually by setting its peak intensity to 1.

We aimed to extract CTAB while maintaining the phase-distinction. CTAB has a low solubility in oils, but alcohols and water can solubilize the charged amphiphile well.[49,50] We used the lipophilic 1-octanol, which was saturated with water to prevent dissolution of the aqueous bijel phase. Dr. M.F. Haase had successfully used this procedure in large domain bijels (**Figure 16**a), but the method had not yet been tried for the 1-propanol/DEP/water system. The removal of surfactant could be monitored with confocal microscopy. Due to the adsorption of Nile red to CTAB at the nanoparticle surface, there is a second region of fluorescence (550 – 700 nm) in

addition to that of this dye in hexane (Figure 16b). Therefore, the removal of surfactant should lower fluorescence at these wavelengths. This trend can be seen in Haase's micrographs, where the intensity of the particle channel decreases after washing with octanol. Furthermore, TEOS-treatment led to the deposition of silica. Therefore, more surface was present for Nile red to adsorb to, which increased the signal intensity compared to fresh, untreated fibers in Haase's findings. Although the surfactant adsorption proceeds differently in our 1-propanol system, we expected the procedure to yield similar results, since our system uses the same TMA nanoparticles and CTAB.

4.2.3. TEOS-treatment in dodecane

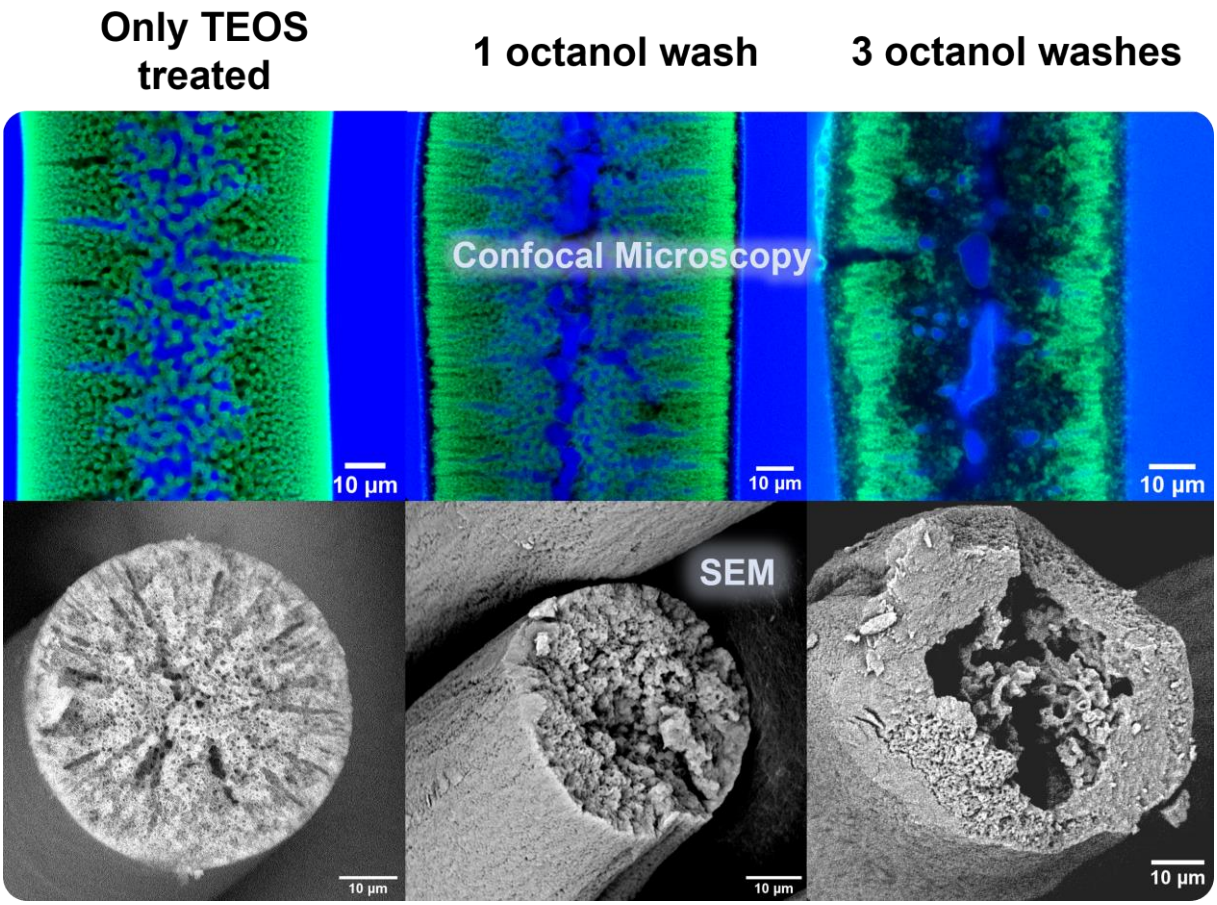

Figure 17: Scanning Electron Microscopy (SEM) and confocal micrographs of fibers which have undergone octanol wash. Dodecane was the solvent during TEOS-treatment.

We printed bijel fibers with the structure shown in Figure 13. In contrast to earlier publications where TEOS was included in the ternary mixture,[19] we added the reagent to the oil phase post-

fabrication via diffusion from the ambient liquid, followed by the octanol wash. The washing treatment was characterized through confocal and scanning electron microscopy (SEM).

Hexane generally leaked into the water channel in TEOS-treated fibers during confocal imaging. This phenomenon is discussed in detail in section 4.3. The introduction of a single octanol wash immediately destroyed the bicontinuity (**Figure 17**). Subsequent washes resulted in a hollow interior, which was surrounded by an exterior of fused silica. The dislocation of particles from the interface indicated that the octanol wash changed the particle wettability and CTAB was extracted. Importantly, it also suggested that the crosslinking was unsuccessful, otherwise the interconnected scaffold would have been maintained. Paradoxically, when unwashed fibers were dried, the particle scaffold remained intact even without the aid of interfacial tension. Possibly the particle aggregation inside the oil channel, along with minor silica deposition, created a weakly reinforced gel. This structure could withstand the capillary stresses of solvent evaporation, but not the change in wettability upon removal of the surfactant.

4.2.4. TEOS-treatment in mineral oil

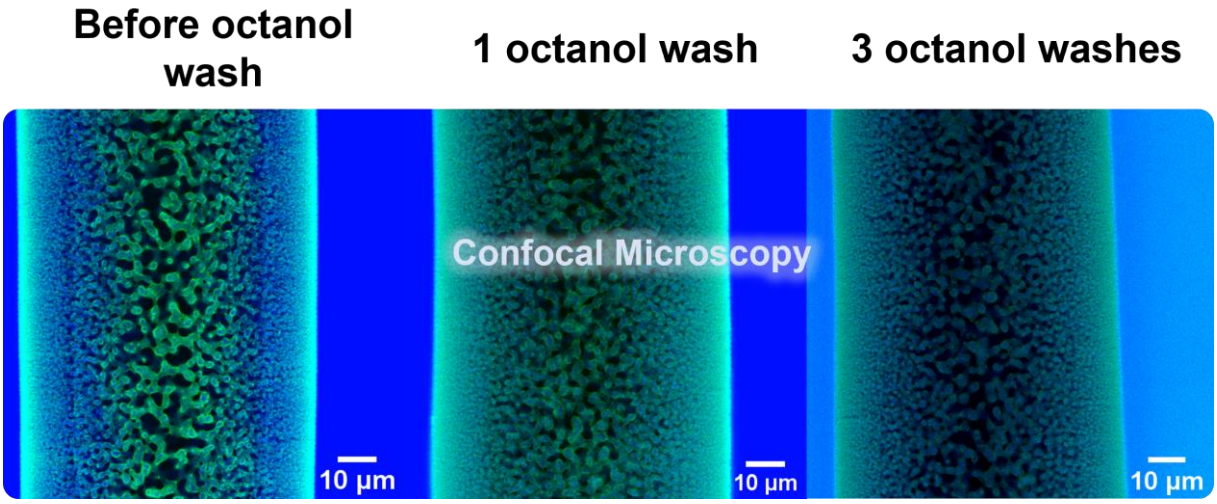

Figure 18: Confocal micrographs of fibers before and after the octanol wash. During TEOS-treatment mineral oil was the solvent.

As will be explained in chapter 4.3, we changed the solvent in TEOS-treatment from dodecane to mineral oil. We varied the concentration between 1, 3 and 5 wt.% and treated the fibers for 8, 18 or 75 hours. Surprisingly, the scaffold remained intact, and we no longer observed the thick crust on the surface (**Figure 18**). Moreover, none of the fibers became hollow when

mineral oil was used. Chapter 4.3.4 describes the reasoning behind these observations. We found that the optimal treatment was 3 wt.% TEOS for 18 hours (appendix 4).

Unfortunately only a fraction of the fibers had the bicontinuous structure shown above. The vast majority showed hexane-to-water channel leakage (**Figure 19**). Nevertheless, the particles remained in the scaffold without the aid of an oil-water interface, which tells us that TEOS-treatment in mineral oil successfully crosslinks the nanoparticles. The number of octanol washing steps did not influence the degree of leakage. Hence we concluded that it is not the removal of surfactant which causes hexane to leak into the water channel. Consequently, we quantified the amount of CTAB via the fluorescence intensity of the nanoparticles, in fibers that did not show hexane-to-water channel leakage (section 4.2.5).

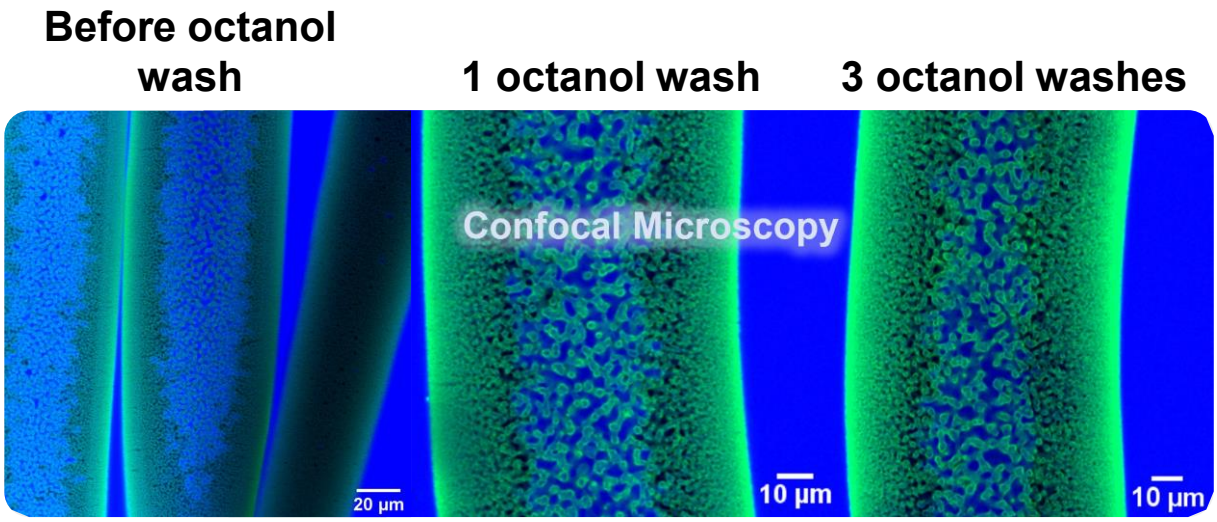

Figure 19: Confocal micrographs of octanol-washed fibers which show hexane-to-water channel leakage. Mineral oil was the solvent during TEOS-treatment.

4.2.5. Quantitative analysis of CTAB removal

Particles were expelled from the fiber upon washing with octanol when they were insufficiently crosslinked (Figure 17). The loss of interfacial activity signaled a change in particle wettability and hence the removal of the amphiphilic CTAB. We quantified this removal with confocal fluorescence microscopy, where a spectral scan (460 - 770 nm) was recorded at the equatorial plane of bijel fibers submerged in a solution of Nile red in hexane. This dye fluoresces at longer wavelengths when it is adsorbed to CTAB at the nanoparticles than when it is dissolved in hexane (Figure 16b). The extraction of CTAB by 1-octanol only decreases the particle emission

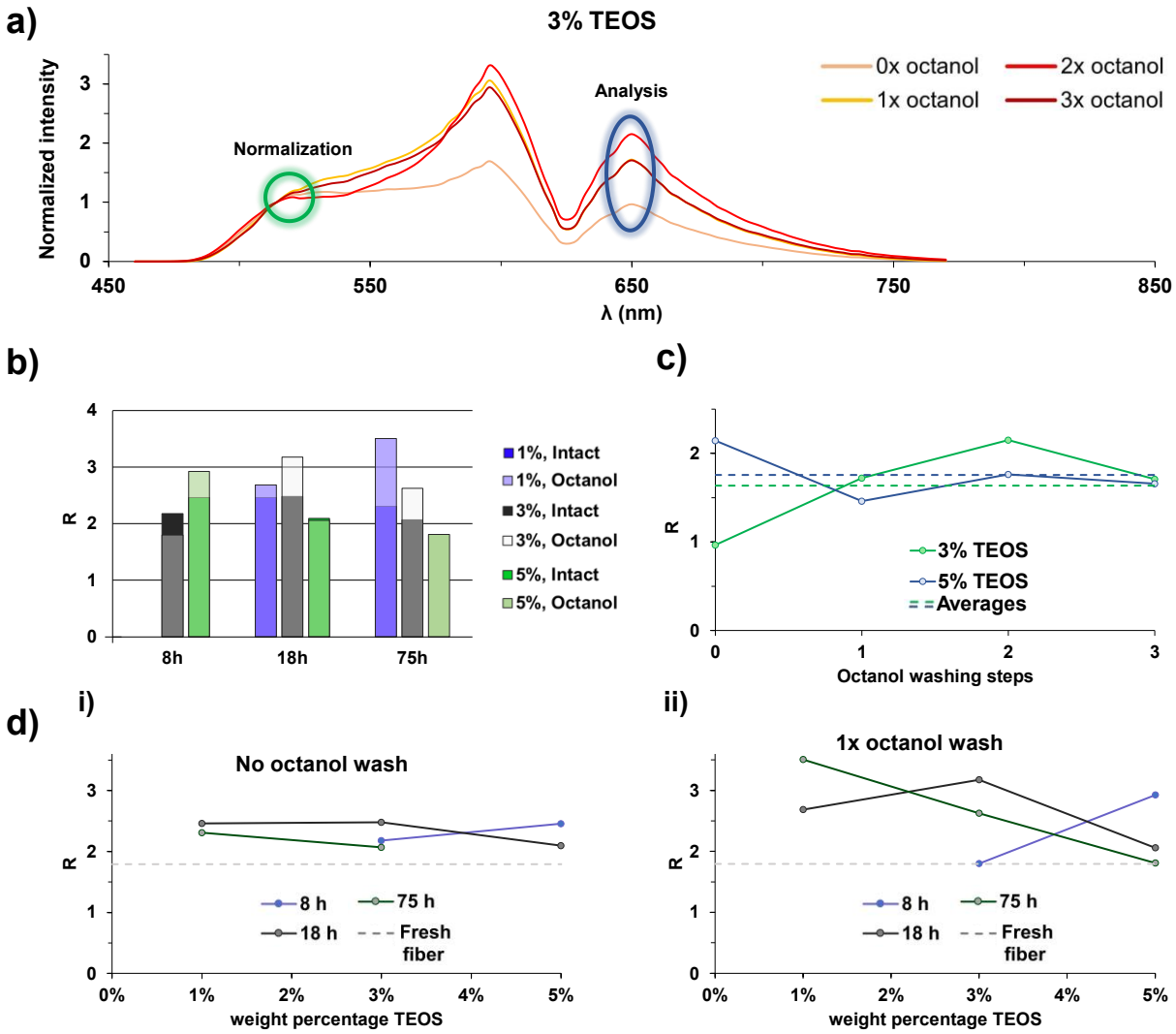

Figure 20: (a) Spectral scan of Nile red fluorescence in a bijel fiber before and after octanol washes. *R* is the ratio between the particle peak at 650 nm and the hexane peak at 515 nm (formula 4.1), which was used for subsequent analysis. (b) Before (*Intact*, dark tones) and after 1 octanol washing step (*Octanol*, light tones), at different strengths of TEOS-treatment. (c) Dependence on the number of octanol washing steps after 18 hours of TEOS treatment, dashed lines indicate the averages. (d) Dependence on the duration and concentration of TEOS crosslinking before (i) and after (ii) washing fibers with octanol. The dashed line is the intensity of freshly extruded, untreated fibers.

above 550 nm. Because the fluorescence peak in hexane is not affected by the amount of CTAB, we normalized the emission spectra with respect to the 515 nm oil-channel peak. We monitored

the amount of CTAB via the ratio *R*:

$$R = \frac{I_{650\,nm}}{I_{515\,nm}} \tag{4.1}$$

where I_{650nm} is the peak emission of the particles, and I_{515nm} that of the reference peak. Surprisingly, R either stayed the same or increased slightly after washing with octanol (**Figure 20**a, b; appendices 5, 6). The specific number of washing steps made no significant difference (Figure 20c). If a significant amount of CTAB were removed, we should observe a noticeable downward trend with the number of washes. Therefore, the amount of removed CTAB was likely insufficient to noticeably decrease the emission signal.

We also analyzed the effect of the concentration and duration of TEOS treatment on the particle fluorescence. We expected the particle emission to increase with stronger TEOS-treatment, analogous to Haase's findings. The hypothesis was confirmed by our experimental findings (Figure 20d). We suspect that R increased post-TEOS-treatment due to the deposition of new silica. The larger surface area to which Nile red could adsorb subsequently increased the particle fluorescence. Interestingly, the specific duration or concentration of TEOS did not lead to significant changes in the recorded emission. Possibly, initial silica deposition occurred rapidly and lowered the porosity of the interfacial particle scaffold. Consequently, the decreased contact between the oil and aqueous phase slowed down the hydrolysis of the oil-soluble TEOS, and less silica was condensed onto the particles over time.

Differences in the particle modification during STrIPS could explain why the procedure was successful in large domain bijels. Haase used a ternary mixture with 2-propanol as solvent, which diffuses into the continuous phase more slowly than 1-propanol. Therefore, the in-situ particle modification would also be slower, and there should be less surfactant at the particle surface in the final bijel structure.

Overall, we found no dependence of the fluorescence intensity on either the strength of TEOS-treatment or on the number of octanol washes. Possibly, protonation of surface hydroxyl groups could aid the removal of the cationic surfactant. The statistical accuracy of the findings is low due to the small sample size, which resulted in a large spread in the data. Additionally, octanol residue could have corrupted the recorded particle intensities, since Nile red fluoresces at comparable wavelengths in alcohol.

4.3. Hexane-to-water channel leakage

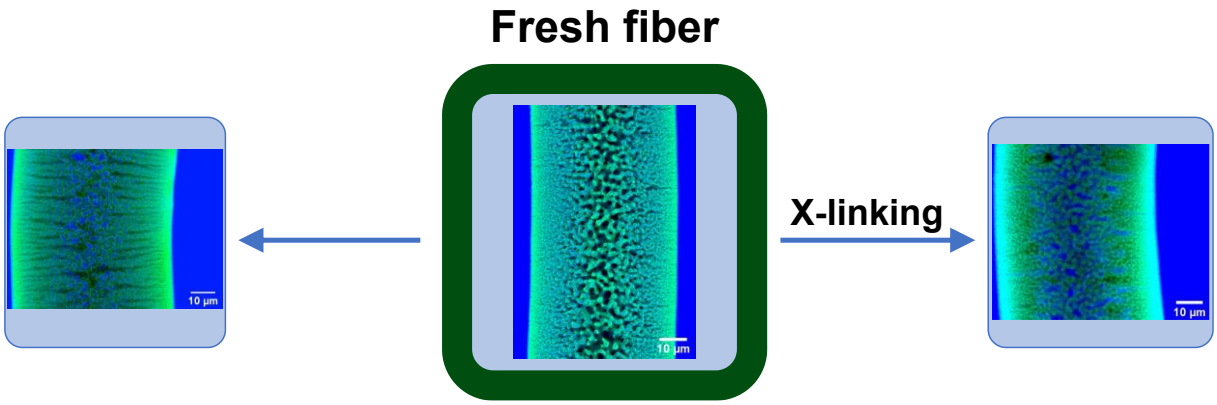

Figure 21: Confocal micrographs showing hexane-to-water channel leakage in fresh (left) and TEOS-treated fibers (right).

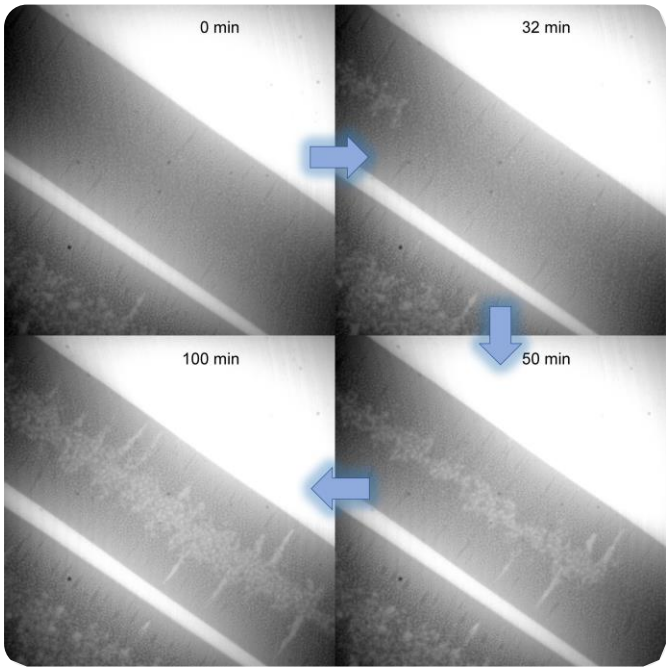

Figure 22: Timelapse of hexane-to-water channel leakage in TEOS treated fibers (A.J. Sprockel, January 2021).

Over time, hexane droplets appeared in the water channel during imaging (**Figure 21**). The leakage originated at the endings, where the water channel is exposed to the ambient oil. It spread throughout the bijel via the large pores in the center (**Figure 22**). The ratio oil : water volume is 1 in fresh fibers, but can increase up to 12 over time (appendix 7). This hexane-to-water channel leakage occurred more rapidly in TEOS-treated fibers. Since March 2021, the hexane flooding has worsened significantly. We switched from fragments to intact fibers to

decrease the relative area of the fiber endings, which serve as a leakage site. Regrettably, the hexane leakage remained. Several parameter studies were carried out to locate the cause of the fiber deterioration.

4.3.1. Oil type and longevity

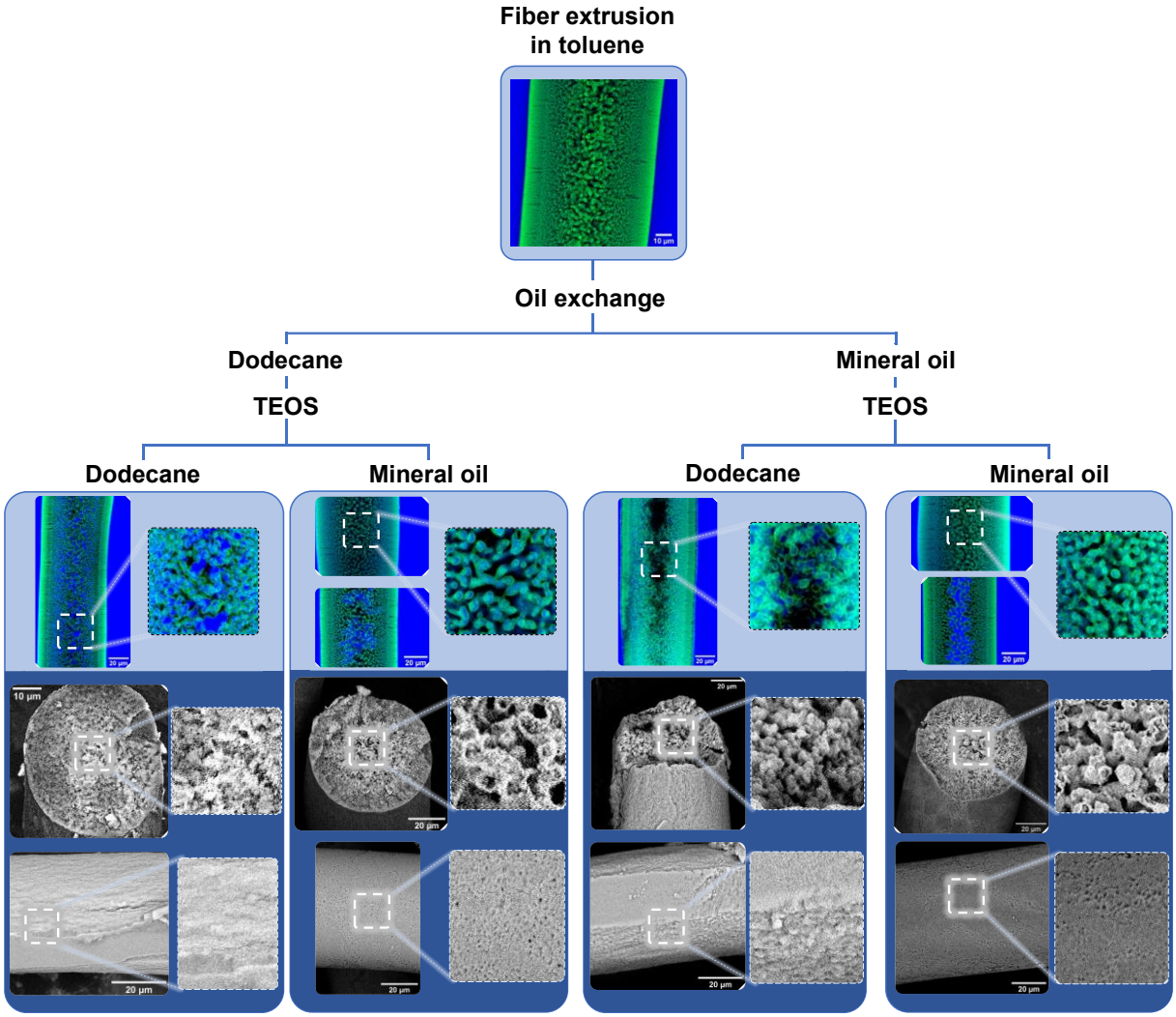

Figure 23: Fibers were extruded in toluene, which was immediately exchanged for either dodecane or mineral oil. During TEOS treatment, we also varied the solvent between these two.

Bijels were extruded in toluene and are typically stored in the more hydrophobic *mineral oil*. We used dodecane instead, which is of similar hydrophobicity, but lower viscosity. However, when the ambient toluene was exchanged for dodecane, the fibers started to vibrate. The movement could be caused by diffusiophoresis, induced by concentration gradients.[90] The mechanical stress might cause ruptures, through which hexane could leak into the water channel during imaging. The vibrations were not seen in mineral oil, probably due to its high viscosity.

We expected that the use of mineral oil would resolve the hexane-to-water channel leakage. Surprisingly, it was not the vibrations which caused the structural degradation, but the solvent choice during TEOS-treatment (**Figure 23**). Crosslinking in dodecane led to a fused scaffold, clogged surface pores and the formation of a thick crust on the exterior of the fiber. None of these issues were seen when mineral oil was used, aside from the ever-present hexane-to-water channel leakage.

4.3.2. Water content of the oil

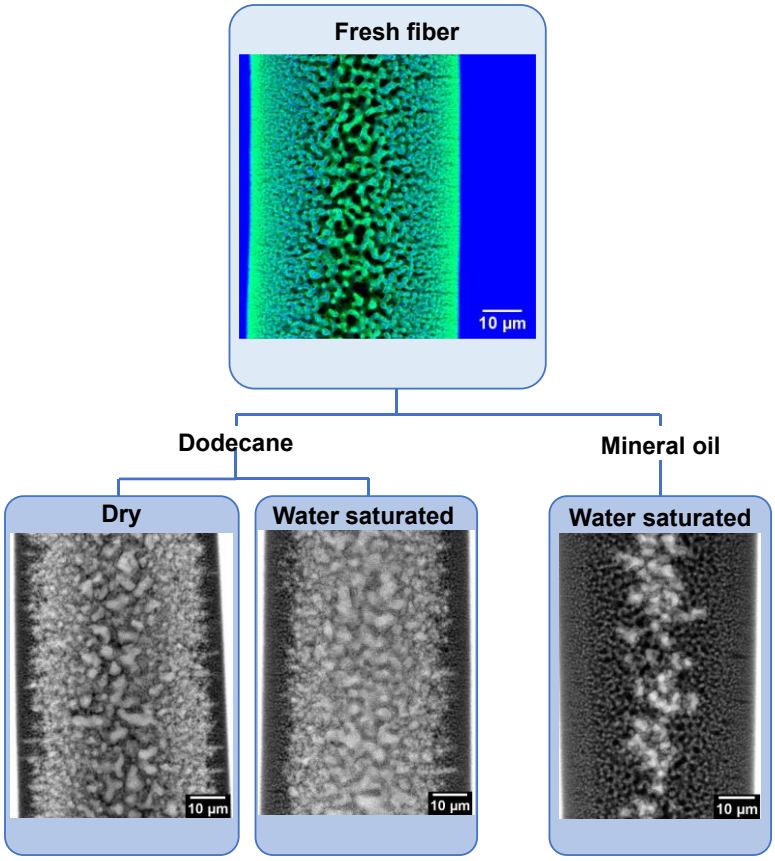

Figure 24: The water content of dodecane was varied during TEOS-treatment, and compared to fibers in mineral oil.

Subsequent experiments were performed to find out why mineral oil offered such an improvement over dodecane. Because the reaction of TEOS with the nanoparticles consists of a hydrolysis and a condensation step, the water content should influence the kinetics. We hypothesized that dodecane contained more water than mineral oil. The deposition of silica was then rapid enough to clog the surface pores at an early stage, and the reagent could no longer diffuse into the fiber. The interior would not be reinforced, and would be washed away with

octanol. All silica would be deposited on the outer surface, which could explain the thick crust on the fiber exterior. To test the hypothesis we varied the water content of both solvents. In dodecane, all TEOS treated fibers showed a high degree of hexane-to-water channel leakage (**Figure 24**). When mineral oil was used, hexane only leaked into the large central pores. The use of mineral oil therefore did not fully resolve the hexane leakage.

4.3.3. Weak points and structural deformations

The fibers often contained dilations, which ruptured upon TEOS-treatment (**Figure 25**a). Additionally, the radial channels appear to be weak points which can fracture (Figure 25b). A.J. Sprockel found the surface expulsions could be removed by increasing the flow rate of the continuous phase. The steep divergence in velocity translates to a high shear stress on the surface of the ternary flow. We suppose the shear is necessary to counteract the osmotic pressure caused by the high concentration of nanoparticles inside the ternary mixture.

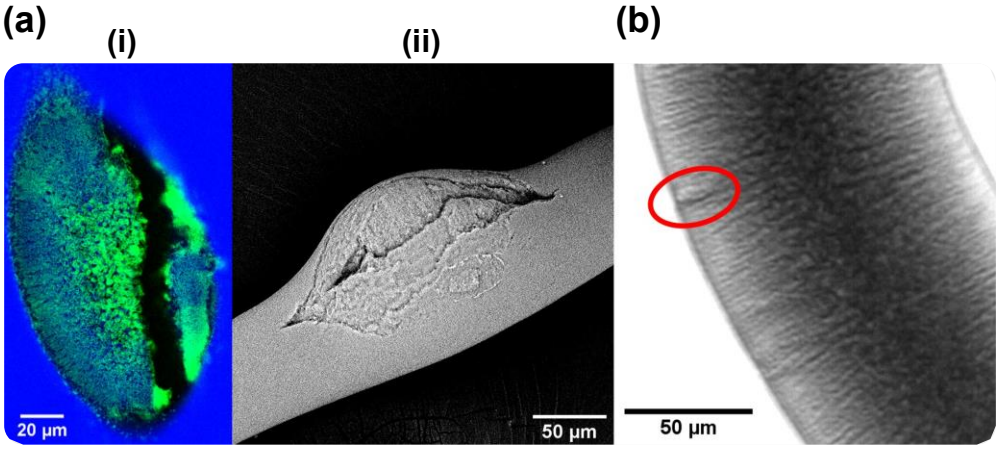

Figure 25: Structural defects in bijel fibers, (a) Ruptured fiber around a surface expulsion, (i) confocal microscopy, (ii) SEM, (b) Brightfield micrograph of a fracture at a radial channel.

To remove the dilations, we tuned the flow rate of the continuous phase relative to that of the ternary mixture, and the printer speed of the nozzle (**Figure 26**). Ideally, the speed of the nozzle movement should match that of the fluid flow at the orifice. Otherwise, the fibers fragment due to the large shear stress caused by the sudden change in velocity. Upon increasing the flow rate and the printer speed, the frequency of the dilations decreased. Finally, the dilations were absent when the nozzle was moved above 22 L.U. (Lego Units) and the flow rate of the continuous phase was 10 mL/h.

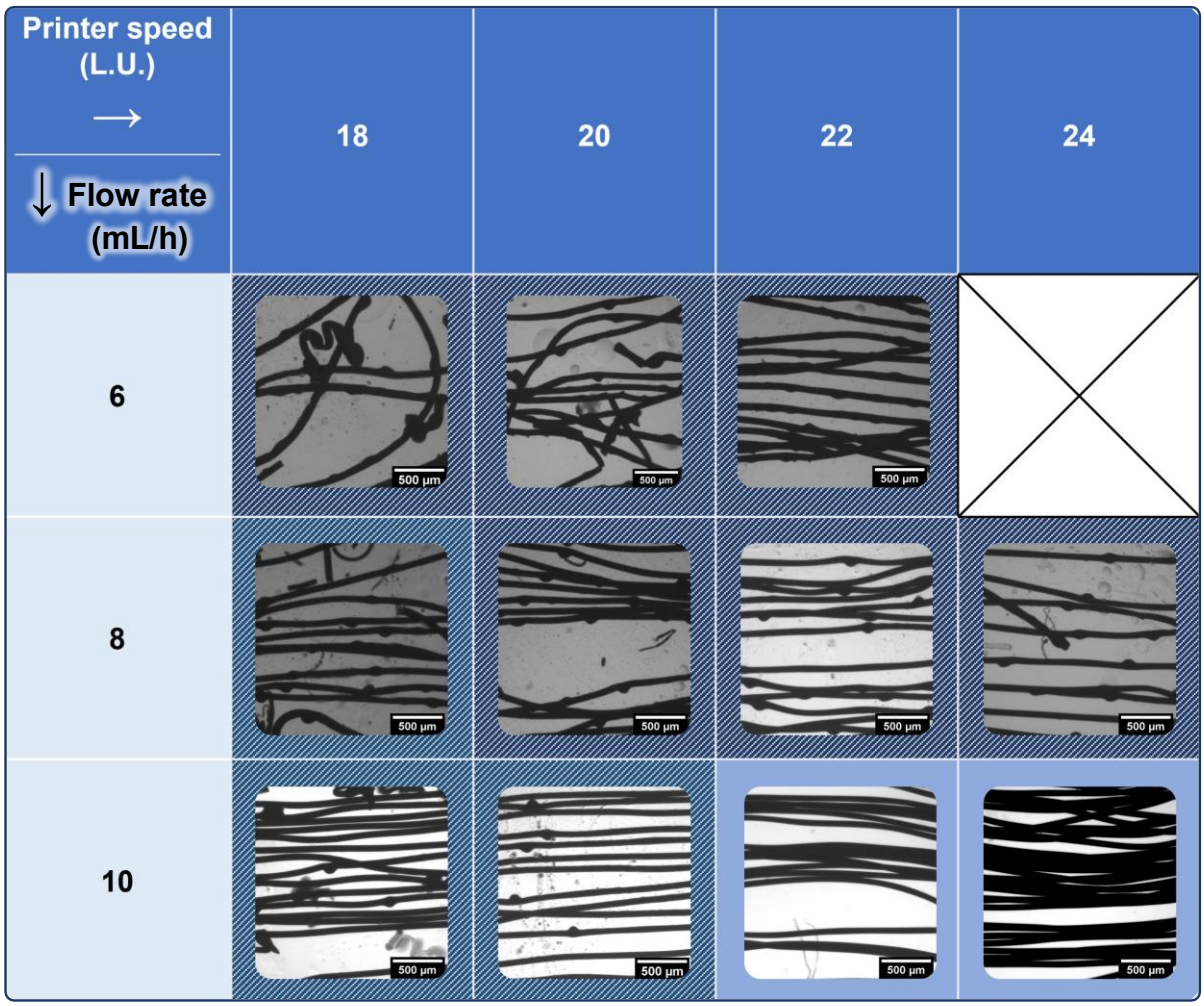

Figure 26: Extrusion parameter study for printing speed (1 L.U. = 10 °/s) and flow rate of the continuous phase. The ternary flow rate was constant (0.5 mL/h). The light blue cells correspond to fibers with a smooth, expulsion-free surface. Shaded areas correspond to expulsions on the fiber surface. The cross indicates that the fibers fragmented.

The exact cause of radial channel formation is still unknown, but they generally appear at higher CTAB concentrations (Figure 14). These hollow pores lack the support of the particle scaffold and could rupture in the more brittle TEOS-treated fibers. We intentionally fabricated fibers with dilations and radial channels to compare the effects of these parameters. Firstly, the removal of dilations drastically reduced the degree of hexane-to-water channel leakage, but did not fully resolve it (**Figure 27**). Presumably, the severe ruptures expose the water phase to the ambient oil, and serve as leakage sites. Secondly, radial channels are large-diameter pores which rapidly filled with hexane. Nevertheless, the leakage did not spread into the smaller domains, in contrast to the intense leakage with fiber dilations.

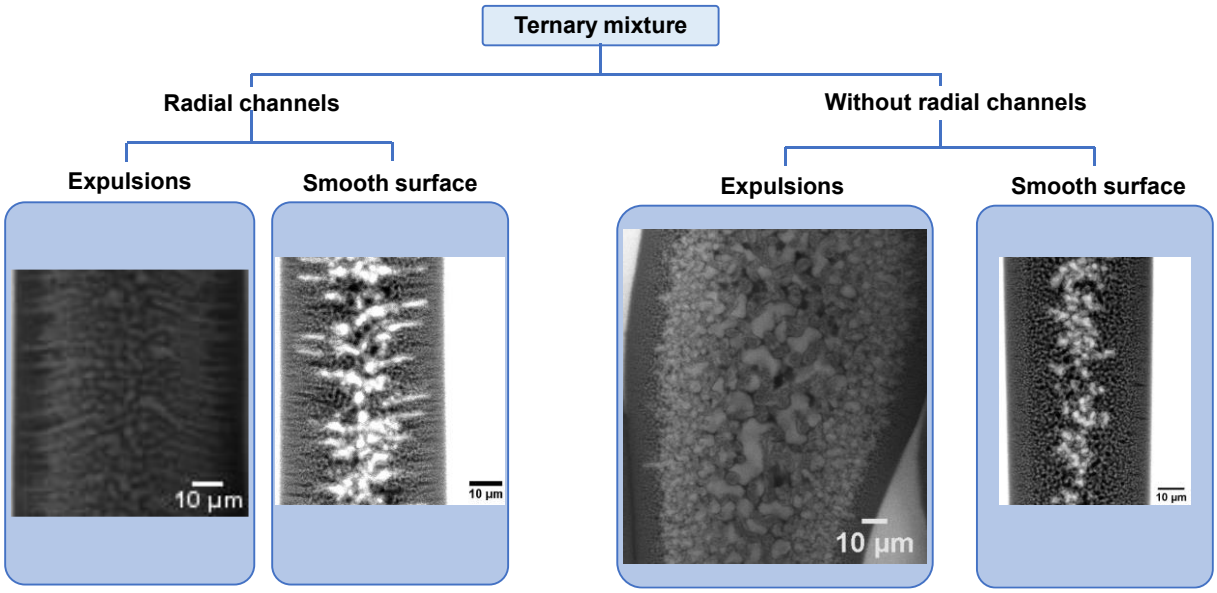

Figure 27: Confocal micrographs of the oil channel. To find out the cause of the structural defects, fibers were prepared with and without radial channels. The extrusion parameters were also varied to induce surface expulsions and to assess their influence on hexane-to-water channel leakage.

4.3.4. Particle hydrophobicity

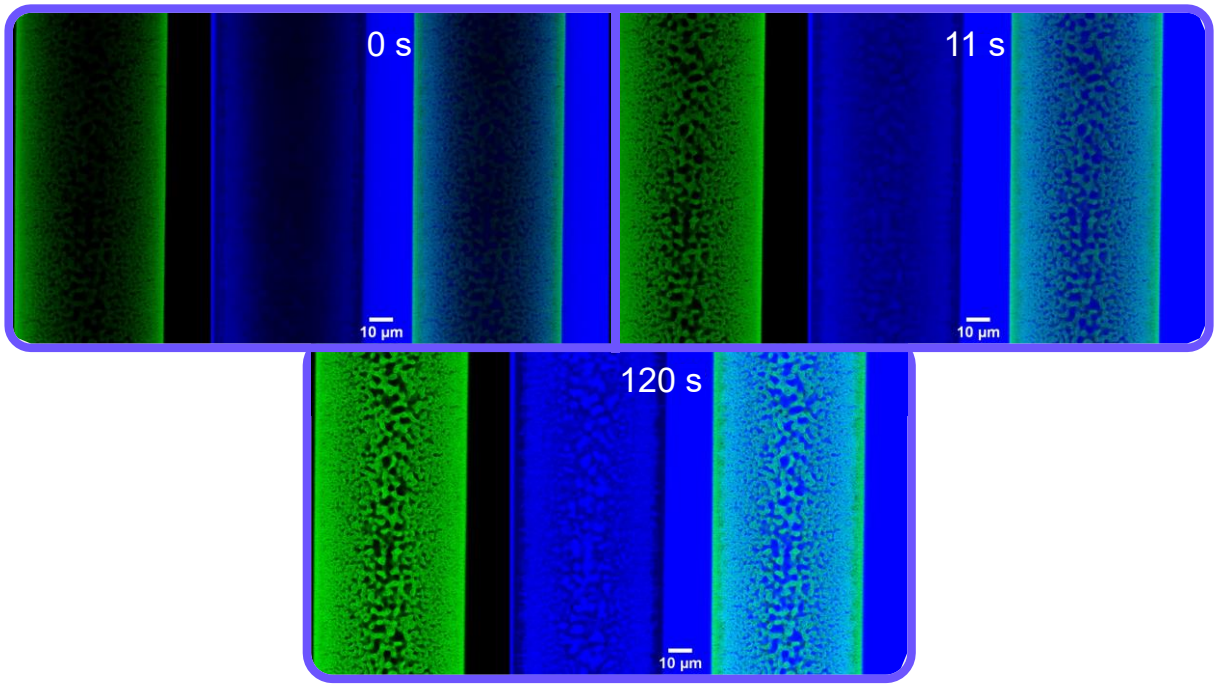

Figure 28: Timelapse of a fiber after application of Nile red and hexane. The ambient phase was changed from mineral oil to Nile red in hexane at t = 0 s. The intensity increased over time due to the diffusion of dye into the fiber.

To gain insight into the hexane-to-water channel leakage, we set out to monitor the process over time. The ambient mineral oil was replaced with Nile red in hexane at the start of imaging (**Figure 28**). We expected to observe the advance of oil throughout the water channel, but the oil fluorescence was immediately visible across the entire fiber at the moment of application. The instantaneous emission from the water channel tells us that the dye could simply diffuse into a channel which was already occupied by oil. Therefore, the flooding phenomenon is not exclusive to hexane, and storage on mineral oil also spawns oil-to-water channel leakage.

During STrIPS, the removal of solvent triggers phase separation, as well as the electrostatic adsorption of CTAB onto the nanoparticles. The surfactant concentration is tuned such that the particles are neutrally wetting at the moment of interfacial jamming (**Figure 29**a). However, more 1-propanol diffuses out of the fiber after this point, and CTAB continues to adsorb. The particle aggregation in the oil channel showed that the in-situ modification eventually renders the particles hydrophobic. The particle-water interface results in a decrease in entropy due to the hydrophobic effect, which makes the arrangement energetically unstable.[91] This thermodynamic instability would be resolved via oil-to-water channel leakage, after which solely the favorable oil-particle interactions remain (Figure 29b). Only a minimal volume of water has to be dissolved at one time because the oil spreads slowly. This water could be redeposited elsewhere, such that the aqueous content of the oil never exceeds the maximum solubility.[92–97] Therefore, oil-to-water channel leakage should be energetically favorable, since water droplets present a lower surface area than the aqueous phase inside a bijel. We did not observe these droplets since the total volume of the aqueous phase is below 10 µL (appendix 8). Likely, the oil leakage originates at points where the water phase is exposed to oil, for instance at ruptures.

Originally our group believed the oil leakage was unique to hexane. Mineral oil was supposedly too hydrophobic to dissolve the water channel. As we have shown, the hydrophobic character of the particles cause any oil to eventually leak into the water channel. The aqueous phase is dissolved and likely redeposited outside the bijel fiber, to reduce the unfavorable water-particle interactions. The oil-leakage is not observed as readily in mineral oil as in hexane or dodecane, because the liquid flows more slowly due to its high viscosity. Since TEOS-treated fibers were at least a day old at the point of confocal analysis, mineral oil had already leaked into the large central pores of the water channel. Therefore, we commonly saw oil inside TEOS-treated fibers during imaging. Importantly, dodecane and hexane are over 20 times less viscous, which caused

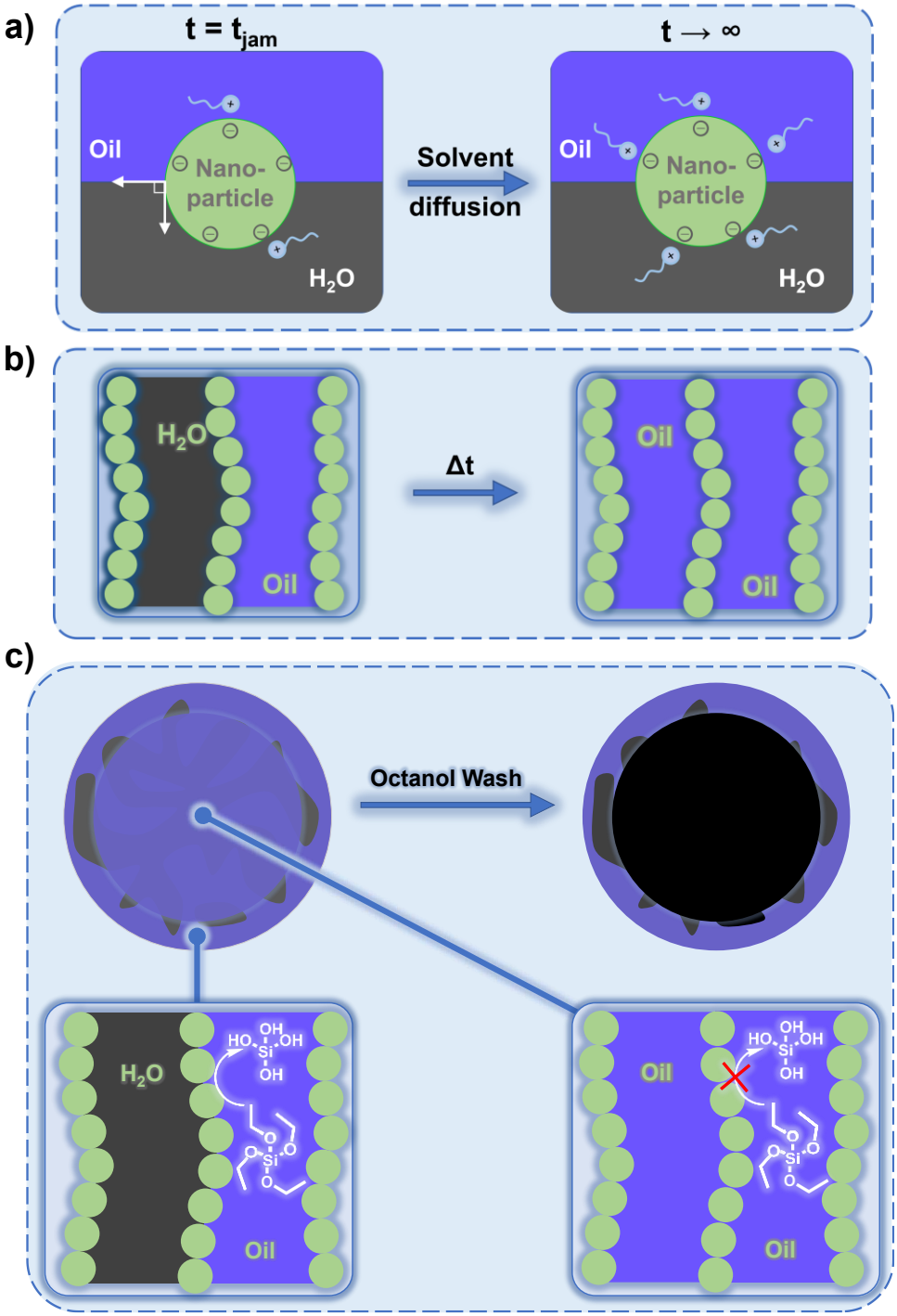

Figure 29: (a) Particles are neutrally wetting at the stage of interfacial jamming. The further removal of solvent increases surfactant adsorption and renders the particles hydrophobic. They cannot change their contact angle as that would expose more oil-water interface. (b) Over time, oil floods the water channel to remove the energetically unfavorable water-particle interactions. (c) When TEOS treatment is done in dodecane, the center of fibers consists entirely of oil due to the rapid oil-to-water channel leakage, which prevents TEOS hydrolysis. Towards the surface, the scaffold is reinforced since the narrow pores still contain water due to the high Laplace pressure. After octanol wash, the unfortified interior is flushed away.

these oils to replace the aqueous phase more rapidly. When TEOS was dissolved in dodecane, the oil leaked into the central water pores before TEOS had sufficiently been hydrolyzed (Figure 29c). Subsequently, the particles were not fixed inside the scaffold and were swept from the interface upon removal of the surfactant. The oil-water interface is necessary to crosslink the nanoparticles, as the aqueous content of water-saturated oils is insufficient to lead to TEOS hydrolysis. Possibly, we could forego TEOS treatment and directly use alkyl trichlorosilanes to form an interconnecting, hydrophobic particle network for reinforcement.[18] The rapid reaction should facilitate phase-selective hydrophobization before the onset of oil-to-water channel leakage. Finally, the electro-osmotic flow rates measured by A.J. Sprockel at pH 9 indicate a zeta potential of around -40 mV. The large potential suggests that the applied electric field has removed the cationic CTAB from the water channel.[90] Interestingly, these fibers did not show oil-to-water channel leakage, since any oil droplets were likely flushed out with the flow.

Unfortunately, it seems the structure of small-domain bijels is unstable over time. The further depletion of 1-propanol after the point of interfacial jamming in STrIPS renders the particles hydrophobic, and the water-particle interactions come at a high energetic cost. Over time, this instability leads to structural degradation. Possibly, electro-osmosis restores the bicontinuity. The implementation of this technique pre-hydrophobization should aid in the fabrication of bijels as Janus porous media.

4.3.5. Additional contributing factors

Where the oil-to-water channel leakage was initially only seen in hexane (Figure 22), we now also face this issue with fibers stored in mineral oil. Additionally, the surface expulsions and particle aggregation in the oil channel have worsened, and there is a large radial pore size gradient. In March 2021 we were unable to fabricate bijels with LUDOX TMA particles, but the manufacturer notified us that the issues they faced setting up the processing plant had been resolved since then. Nevertheless, the particles aggregate more strongly, the pH drifts more rapidly and there is a steeper radial pore size gradient compared to older TMA batches. A more profound understanding of the Ludox TMA surface chemistry would allow us to more effectively address these issues.

4.4. Phase-selective hydrophobization

Initial experiments showed that fibers treated with HTES remained hydrophilic (section 4.2.1). Therefore, we included an octanol washing step before the hydrophobization reaction. Upon rewetting of dried, functionalized fibers, water should only fill the untreated channel. On the other hand, oil would be free to fill the hydrophobized pores. The application of liquids in this sequence should reconstitute the original bijel phase system. Unfortunately, oil had flooded the water channel pre-treatment via the aforementioned oil-to-water channel leakage. Only the narrow pores close to the surface could maintain their water content due to the high Laplace pressure. As a consequence, we expected both pore systems to be hydrophobized by the oil-soluble reagent. Therefore, most of the fiber should fill with oil upon rewetting. Nonetheless, we could show proof of concept if the narrow channels close to the surface would contain distinct phases after reconstitution.

We used octadecyltrichlorosilane (OTS, 1 wt.%, 18 h) to hydrophobize the oil channel. The use of an ethoxysilane with the same alkyl chain would allow for a meaningful comparison between substituents. However, octadecyltriethoxysilane could not be used due to limitations in the chemical supply. Therefore, our options were limited, so we decided to use HTES at higher concentrations than before (5 wt.%, 18 hours). This compound had been used successfully to hydrophobize silica surfaces.[98] Subsequently, we characterized the hydrophobization treatment with confocal microscopy. Dried, functionalized fibers were wetted with Nile red in hexane or aqueous rhodamine-B as references. Unexpectedly, both dyes adsorbed onto the particles so strongly that there was no fluorescence recorded in the liquid (appendix 9). The dye drainage was especially unusual for Nile red, since the oil phase fluoresced before the fibers were dried. Without a fluorescent oil phase, confocal microscopy cannot be used to analyze the reconstitution of phase-selectively hydrophobized bijels. The adsorption of Nile red onto the nanoparticles is facilitated by CTAB. Therefore, the complete removal of CTAB should eliminate the dye drainage from the constituent phases.

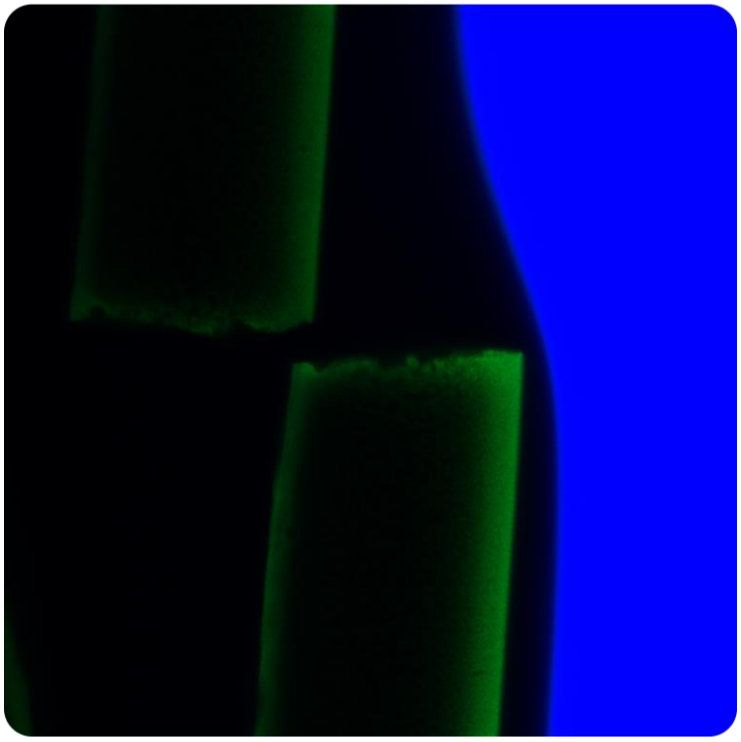

Figure 30: Confocal micrographs of fibers after treatment with HTES. The fibers were brought into contact with a water droplet (black) and wetted readily. The oil (blue) was not able to reach the fiber (green).

To test the hydrophobicity, we again introduced a water droplet to the fiber surface (section 4.2.1). Regrettably, OTS had formed a thick hydrophobic residue on the fiber surface, which was impenetrable for the dye (appendix 9). Nonetheless, the fast reaction of OTS highlighted that it is unnecessary to remove CTAB to hydrophobize fibers. Moreover, when octanol-washed fibers were treated with HTES, they still wetted readily upon contact with a water droplet (**Figure 30**). This observation suggests that also the findings from section 4.2.1 were not caused by CTAB interference, but likely due to the slow hydrolysis of the ethoxy substituents. To increase the hydrolysis rate of HTES, a more extreme pH could be used.[64] Alternatively, a lower OTS concentration, or shorter reaction time, should prevent the formation of the thick residue. It should also be worthwhile to use methoxysilanes, which react more readily than ethoxysilanes.[18] Most importantly, the oil-to-water channel leakage needs to be resolved. It is impossible to fabricate Janus bijels without a fully bicontinuous network of oil and water.

5. Conclusions and outlook

Hydrogen fuel cells are essential in the transition to sustainable electricity, since the output of renewable energy sources fluctuates over time.[3] During moments of peak production, excess green electricity could be stored in the form of hydrogen via water hydrolysis. The electricity can be reclaimed with the use of proton-exchange membrane fuel cells (**PEMFC**s).[5] In these hydrogen fuel cells, a *gas diffusion layer* (**GDL**) is essential to drain the electrochemically formed water.[7] To this end, we propose a phase-selectively hydrophobized *bicontinuous interfacially jammed emulsion gel* (**bijel**). The hydrophobization of solely the oil channel would create a Janus porous material with separate pathways for diffusion of oxygen and water. The interwoven, bicontinuous network of channels with opposite wettability offers intimate contact between pore systems of opposite wettability.[12,44,55] Furthermore, bijels would become the first material to extend the asymmetric Janus character to 3 dimensions.[22] During this project we addressed several key issues in the production process of such a Janus porous material.

We used *Solvent Transfer Induced Phase Separation* (**STrIPS**) for the continuous fabrication of porous bijel-based templates with sub-micron domains.[15,17] We have shown that bijels cannot be turned into Janus porous media unless the oil-to-water channel leakage is resolved. The phase-distinction should be maintained, since otherwise both pore systems are hydrophobized. The leakage is caused by the hydrophobic particle character, which the excess surfactant adsorption in STrIPS inherently imparts onto their surface in the 1-propanol system.[16,17] The hydrophobic effect makes the water-particle interactions energetically unfavorable. Oil-to-water channel leakage therefore occurs spontaneously, since it decreases the water-particle interfacial area. The flooding of the water channel was delayed in viscous oils due to their slow flow behavior. Possibly, the application of an electric field could remove the cationic surfactant, and electro-osmotic flow would expel any residual oil droplets from the water channel.

Importantly, fresh fibers lack the mechanical strength to withstand the capillary stresses of solvent evaporation. Treatment with *tetraethylorthosilicate* (**TEOS**) in mineral oil successfully reinforced the structure through the deposition of silica.[19] However, rapid oil-to-water channel leakage prevented the hydrolysis of TEOS when dodecane was used as a solvent. Additionally, silanes were used to alter the wettability of the particle surface. Contrary to expectation, the fibers initially remained hydrophilic after treatment with *hexyltriethoxysilane* (**HTES**, 1 wt.%,

18 hours). We suspected that the surfactant *cetrimoniumbromide* (**CTAB**) interfered with the reaction, as this had been shown in literature.[89] Hence, we expected that the removal of surfactant would improve the effectiveness of the hydrophobization treatment. Therefore, we attempted to extract CTAB with water-saturated 1-octanol. Unfortunately, we observed no decrease in the emission peak which was associated to particle channel fluorescence. Although a larger sample size is needed to increase the statistical relevance, these initial experiments suggest that octanol alone does not remove a significant amount of CTAB from the particle surface in small-domain bijels. Possibly, the addition of acid could remove the cationic surfactant via the protonation of superficial hydroxyl groups.

Furthermore, we compared HTES with the more reactive *octadecyltrichlorosilane* (**OTS**). OTS (1wt.%, 18 h) encapsulated the fibers in a thick, hydrophobic residue despite the presence of CTAB. Moreover, even after fibers were washed with octanol, HTES (5 wt.%, 18 h) did not impose a hydrophobic character. Supposedly, it was not CTAB interference that results in poor hydrophobization with HTES, but the ethoxy substituents hydrolyzed too slowly. We could either lower the OTS concentration for a more controlled reaction, or use methoxysilanes, which are of intermediate reactivity.[18] Possibly, we could directly apply hydrophobic trichlorosilanes without TEOS-treatment. The rapid reaction would crosslink the particle network for reinforcement, and impart a hydrophobic character before the phase-distinction is lost through oil-to-water channel leakage.

Problematically, the rewetting of dried fibers led to the complete depletion of Nile red from the oil phase due to the strong adsorption of the dye to the particle scaffold. The adsorption is facilitated by physisorption to CTAB at the particle surface. Because confocal microscopy cannot be used to characterize the Janus character in bijels without oil-channel fluorescence, the removal of surfactant remains important, despite its minor effect on silane condensation.

Lastly, recently acquired batches of Ludox TMA resulted in bijels with a large radial pore size gradient, more severe particle aggregation and rapid oil-to-water channel leakage compared to previously acquired TMA. The differences could be caused by variations in the silica : alumina ratio, due to dissolution of silica and inconsistencies in the production process.[87,88] Additionally, a more clear understanding of the surface chemistry of these nanoparticles would prevent the cumbersome surfactant optimization at the start of each experiment.

Once the phase-selective hydrophobization is applied to bijels, the small-domain structure serves as a template which can be filled with other pairs of immiscible fluids. It could for instance be used to regulate the molecular diffusion in hydrogen fuel cells, and thereby contribute to the development of renewable energy sources.[4] Had he lived to see such a unique application of surface chemistry, Pauli would hopefully change his statement about the diabolic character of interfaces.

6. Acknowledgements

This MSc. project was my first experience at an research department. I am thankful for the chance to do practical work, despite the situation around COVID-19. Of course, I could never have finished this project without the aid of a number of people.

Firstly, I would like to thank Azeem for the daily supervision. He patiently introduced me to the complex system that our group works with. We had many sparring sessions to discuss explanations and theories for the observed phenomena. I want to thank dr. Martin Haase for coming up with this project, and for showing me the standards that are expected in academic research. During our monthly meetings he offered useful advice thanks to his extended knowledge on our field of research. Mariska was always available for questions, and took over the daily supervision when Azeem was absent. Katherine helped me with the experiments on octanol wash, and we exchanged many ideas on what the cause of the oil-to-water channel leakage could be. Alessio supplied me with some data that I used to write this thesis, and his insights helped form some of the theories that are described in it. Of course no practical lab work would be possible without the care of our technicians Dominique and Alex. I also would like to thank everyone in the Haase group for their input during the brainstorm sessions.

Many thanks to Georgios and Henrik for the laughs and ping-pong games we shared during the coffee breaks. I would also like to thank my friends and family for their patience and interest in topics which are far removed from their fields of expertise. Finally, a great thank you to everyone at FCC. I was immediately welcomed into the group on my first day. As an MSc. student, I always felt appreciated and incorporated into the group.

7. Bibliography

(1) Eurostat. Share of energy from renewable sources https://ec.europa.eu/eurostat/databrowser/view/NRG_IND_REN__custom_938915/bookmark/table?lang=en,en&bookmarkId=b365f4d1-44b0-4d52-aee8-a78770914695 (accessed Mar 9, 2022).

(2) Siddi, M. *The European Green Deal: Asseasing Its Current State and Future Implementation*; Finnish Institute of International Affairs, 2020; Vol. 114.

(3) Yekini Suberu, M.; Wazir Mustafa, M.; Bashir, N. Energy Storage Systems for Renewable Energy Power Sector Integration and Mitigation of Intermittency. *Renewable and Sustainable Energy Reviews* **2014**, *35*, 499–514.

(4) Anderson, D.; Leach, M. Harvesting and Redistributing Renewable Energy: On the Role of Gas and Electricity Grids to Overcome Intermittency through the Generation and Storage of Hydrogen. *Energy Policy* **2004**, *32* (14), 1603–1614.

(5) Felseghi, R. A.; Carcadea, E.; Raboaca, M. S.; Trufin, C. N.; Filote, C. Hydrogen Fuel Cell Technology for the Sustainable Future of Stationary Applications. *Energies* **2019**, *12* (23), 4593.

(6) Ijaodola, O. S.; El- Hassan, Z.; Ogungbemi, E.; Khatib, F. N.; Wilberforce, T.; Thompson, J.; Olabi, A. G. Energy Efficiency Improvements by Investigating the Water Flooding Management on Proton Exchange Membrane Fuel Cell (PEMFC). *Energy* **2019**, *179*, 246–267.

(7) Swette, L. L.; Kackley, N. D.; LaConti, A. B. Regenerative Fuel Cells. In *Electrochemical Power Sources: Fundamentals, Systems, and Applications*; Elsevier, 2022; Vol. 1, pp 365–406.

(8) Forner-Cuenca, A.; Manzi-Orezzoli, V.; Biesdorf, J.; Kazzi, M. el; Streich, D.; Gubler, L.; Schmidt, T. J.; Boillat, P. Advanced Water Management in PEFCs: Diffusion Layers with Patterned Wettability I. Synthetic Routes, Wettability Tuning and Thermal Stability. *Journal of The Electrochemical Society* **2016**, *163* (8), F788.

(9) Tranter, T. G.; Boillat, P.; Mularczyk, A.; Manzi-Orezzoli, V.; Shearing, P. R.; Brett, D. J. L.; Eller, J.; Gostick, J. T.; Forner-Cuenca, A. Pore Network Modelling of Capillary Transport and Relative Diffusivity in Gas Diffusion Layers with Patterned Wettability. *Journal of The Electrochemical Society* **2020**, *167* (11), 114512.

(10) Herzig, E. M.; White, K. A.; Schofield, A. B.; Poon, W. C. K.; Clegg, P. S. Bicontinuous Emulsions Stabilized Solely by Colloidal Particles. *Nature Materials* **2007**, *6*, 966–971.

(11) Gross, S. J.; McDevitt, K. M.; Mumm, D. R.; Mohraz, A. Mitigating Bubble Traffic in Gas-Evolving Electrodes via Spinodally Derived Architectures. *ACS Applied Materials and Interfaces* **2021**, *13* (7), 8528–8537.

(12) Clegg, P. S.; Thijssen, J. H. J. Introduction to Bijels. In *Bicontinuous Particle-stabilized Emulsions*; Clegg, P. S., Ed.; Soft Matter Series; Royal Society of Chemistry: Cambridge, 2020; pp 1–33.

(13) Cahn, J. W. On Spinodal Decomposition. *Acta Metallurgica* **1961**, *9* (9), 795–801.

(14) Cai, D.; Clegg, P. S. Stabilizing Bijels Using a Mixture of Fumed Silica Nanoparticles. *Chemical Communications* **2015**, *51* (95), 16984–16987.

(15) Haase, M. F.; Stebe, K. J.; Lee, D.; Haase, M. F.; Stebe, K. J.; Lee, D. Continuous Fabrication of Hierarchical and Asymmetric Bijel Microparticles, Fibers, and Membranes by Solvent Transfer-Induced Phase Separation (STRIPS). *Advanced Materials* **2015**, *27* (44), 7065–7071.

(16) Boakye-Ansah, S.; Khan, M. A.; Haase, M. F. Controlling Surfactant Adsorption on Highly Charged Nanoparticles to Stabilize Bijels. *Journal of Physical Chemistry C* **2020**, *124* (23), 12417–12423.

(17) Khan, M. A.; Sprockel, A. J.; Macmillan, K. A.; Alting, M. T.; Kharal, S. P.; Boakye-Ansah, S.; Haase, M. F. Nanostructured, Fluid Bicontinuous Gels for Continuous Flow Liquid-Liquid Extraction. *Advanced Materials* **2022**.

(18) Arkles, B. Hydrophobicity, Hydrophilicity and Silanes. *Paint and Coatings Industry*. October 2006, pp 114–135.

(19) di Vitantonio, G.; Wang, T.; Haase, M. F.; Stebe, K. J.; Lee, D. Robust Bijels for Reactive Separation via Silica-Reinforced Nanoparticle Layers. *ACS Nano* **2019**, *13* (1), 26–31.

(20) Frijters, S.; Krüger, T.; Harting, J. Parallelised Hoshen–Kopelman Algorithm for Lattice-Boltzmann Simulations. *Computer Physics Communications* **2015**, *189*, 92–98.

(21) Huang, C.; Forth, J.; Wang, W.; Hong, K.; Smith, G. S.; Helms, B. A.; Russell, T. P. Bicontinuous Structured Liquids with Sub-Micrometre Domains Using Nanoparticle Surfactants. *Nature Nanotechnology* **2017**, *12*, 1060–1063.

(22) Yan, L.; Yang, X.; Zhang, Y.; Wu, Y.; Cheng, Z.; Darling, S. B.; Shao, L. Porous Janus Materials with Unique Asymmetries and Functionality. *Materials Today* **2021**, *51*, 626–647.

(23) Sonderegger, B.; Kozeschnik, E. Interfacial Energy of Diffuse Phase Boundaries in the Generalized Broken-Bond Approach. *Metallurgical and Materials Transactions A: Physical Metallurgy and Materials Science* **2010**, *41*, 3262–3269.

(24) Camerin, F.; Zaccarelli, E. Soft Colloids for Complex Interfacial Assemblies. *Proceedings of the National Academy of Sciences* **2022**, *119* (7), e2122051119.

(25) Israelachvili, J. N. *Intermolecular and Surface Forces*, 3rd ed.; Academic Press, 2015.

(26) Zanini, M.; Isa, L. Particle Contact Angles at Fluid Interfaces: Pushing the Boundary beyond Hard Uniform Spherical Colloids. *Journal of Physics: Condensed Matter* **2016**, *28* (31), 313002.

(27) Haase, M. F. Modification of Nanoparticle-Surfaces for Emulsion Stabilization and Encapsulation of Active Molecules for Anti-Corrosive Coatings, Potsdam, 2011.

(28) Aveyard, R.; Clint, J. H.; Horozov, T. S. Aspects of the Stabilisation of Emulsions by Solid Particles: Effects of Line Tension and Monolayer Curvature Energy. *Physical Chemistry Chemical Physics* **2003**, *5* (11), 2398–2409.

(29) Lin, Y.; Skaff, H.; Emrick, T.; Dinsmore, A. D.; Russell, T. P. Nanoparticle Assembly and Transport at Liquid-Liquid Interfaces. *Science* **2003**, *299* (5604), 226–229.

(30) Aveyard, R.; Binks, B. P.; Clint, J. H. Emulsions Stabilised Solely by Colloidal Particles. *Advances in Colloid and Interface Science* **2003**, *100–102*, 503–546.

(31) Ramsden, W. Separation of Solids in the Surface-Layers of Solutions and 'Suspensions' (Observations on Surface-Membranes, Bubbles, Emulsions, and Mechanical Coagulation).—Preliminary Account. *Proceedings of the Royal Society of London* **1904**, *72*, 156–164.

(32) Yang, Y.; Fang, Z.; Chen, X.; Zhang, W.; Xie, Y.; Chen, Y.; Liu, Z.; Yuan, W. An Overview of Pickering Emulsions: Solid-Particle Materials, Classification, Morphology, and Applications. *Frontiers in Pharmacology* **2017**, *8*, 287.

(33) Meissner, J.; Prause, A.; Bharti, B.; Findenegg, G. H. Characterization of Protein Adsorption onto Silica Nanoparticles: Influence of PH and Ionic Strength. *Colloid and Polymer Science* **2015**, *293* (11), 3381–3391.

(34) Maestro, A.; Guzmán, E.; Ortega, F.; Rubio, R. G. Contact Angle of Micro- and Nanoparticles at Fluid Interfaces. *Current Opinion in Colloid & Interface Science* **2014**, *19* (4), 355–367.

(35) Stratford, K.; Adhikari, R.; Pagonabarraga, I.; Desplat, J.-C.; Cates, M. E. Colloidal Jamming at Interfaces: A Route to Fluid-Bicontinuous Gels. *Science* **2005**, *309* (5744), 2198–2201.

(36) Mohraz, A. Simple Shaking Yields Bicontinuity. *Nature Nanotechnology 2017 12:11* **2017**, *12* (11), 1021–1022.

(37) Cai, D.; Clegg, P. S.; Li, T.; Rumble, K. A.; Tavacoli, J. W. Bijels Formed by Direct Mixing. *Soft Matter* **2017**, *13* (28), 4824–4829.

(38) Gibbs, J. W. *Scientific Papers.*; Dover Publications: New York, 1961; Vol. 2 vols.

(39) Favvas, E. P.; Ch Mitropoulos, A. What Is Spinodal Decomposition? *Journal of Engineering Science and Technology Review* **2008**, *1*, 25–27.

(40) Stratford, K.; Adhikari, R.; Pagonabarraga, I.; Desplat, J. C.; Cates, M. E. Chemistry: Colloidal Jamming at Interfaces: A Route to Fluid-Bicontinuous Gels. *Science* **2005**, *309* (5744), 2198–2201.

(41) Lee, M. N.; Mohraz, A. Hierarchically Porous Silver Monoliths from Colloidal Bicontinuous Interfacially Jammed Emulsion Gels. *Journal of the American Chemical Society* **2011**, *133* (18), 6945–6947.

(42) Lee, M. N.; Santiago-Cordoba, M. A.; Hamilton, C. E.; Subbaiyan, N. K.; Duque, J. G.; Obrey, K. A. D. Developing Monolithic Nanoporous Gold with Hierarchical Bicontinuity Using Colloidal Bijels. *Journal of Physical Chemistry Letters* **2014**, *5* (5), 809–812.

(43) Imperiali, L.; Clasen, C.; Fransaer, J.; Macosko, C. W.; Vermant, J. A Simple Route towards Graphene Oxide Frameworks. *Materials Horizons* **2014**, *1* (1), 139–145.

(44) Witt, J. A.; Mumm, D. R.; Mohraz, A. Microstructural Tunability of Co-Continuous Bijel-Derived Electrodes to Provide High Energy and Power Densities. *Journal of Materials Chemistry A* **2016**, *4* (3), 1000–1007.

(45) Santiago Cordoba, M. A.; Spendelow, J. S.; Parra-Vasquez, A. N. G.; Kuettner, L. A.; Welch, P. M.; Hamilton, C. E.; Oertel, J. A.; Duque, J. G.; Meierdierks, E. J.; Semelsberger, T. A.; Gordon, J. C.; Lee, M. N. Aerobijels: Ultralight Carbon Monoliths from Cocontinuous Emulsions. *Advanced Functional Materials* **2020**, *30* (6).

(46) Cha, S.; Lim, H. G.; Haase, M. F.; Stebe, K. J.; Jung, G. Y.; Lee, D. Bicontinuous Interfacially Jammed Emulsion Gels (Bijels) as Media for Enabling Enzymatic Reactive Separation of a Highly Water Insoluble Substrate. *Scientific Reports* **2019**, *9* (1), 6363.

(47) Firoozmand, H.; Rousseau, D. Food-Grade Bijels Based on Gelatin-Maltodextrin-Microbial Cell Composites. *Food Hydrocolloids* **2015**, *48*, 208–212.

(48) Tavacoli, J. W.; Thijssen, J. H. J.; Schofield, A. B.; Clegg, P. S. Novel, Robust, and Versatile Bijels of Nitromethane, Ethanediol, and Colloidal Silica: Capsules, Sub-Ten-Micrometer Domains, and Mechanical Properties. *Advanced Functional Materials* **2011**, *21* (11), 2020–2027.

(49) Smith, G. N.; Eastoe, J. Controlling Colloid Charge in Nonpolar Liquids with Surfactants. *Physical Chemistry Chemical Physics* **2013**, *15* (2), 424–439.

(50) Cheng, X.; Wang, X.; Chen, G. A Convenient and Highly Tunable Way to N-Type Carbon Nanotube Thermoelectric Composite Film Using Common Alkylammonium Cationic Surfactant. *Journal of Materials Chemistry A* **2018**, *6* (39), 19030–19037.

(51) Tran, L.; Haase, M. F. Templating Interfacial Nanoparticle Assemblies via in Situ Techniques. *Langmuir* **2019**, *35* (26), 8584–8602.

(52) Purcell, E. M. Life at Low Reynolds Number. *Citation: American Journal of Physics* **1977**, *45* (3), 3–11.

(53) Gommes, C. J.; Tharakan, J. The Péclet Number of a Casino: Diffusion and Convection in a Gambling Context. *American Journal of Physics* **2020**, *88* (6), 439.

(54) Convery, N.; Gadegaard, N. 30 Years of Microfluidics. *Micro and Nano Engineering* **2019**, *2*, 76–91.

(55) Gould, E. M.; Macmillan, K. A.; Clegg, P. S. Autonomous Analysis to Identify Bijels from Two-Dimensional Images. *Soft Matter* **2020**, *16* (10), 2565–2573.

(56) Lichtman, J. W.; Conchello, J. A. Fluorescence Microscopy. *Nature Methods* **2005**, *2* (12), 910–919.

(57) Marini, A.; Muñoz-Losa, A.; Biancardi, A.; Mennucci, B. What Is Solvatochromism? *Journal of Physical Chemistry B* **2010**, *114* (51), 17128–17135.

(58) Nwaneshiudu, A.; Kuschal, C.; Sakamoto, F. H.; Rox Anderson, R.; Schwarzenberger, K.; Young, R. C. Introduction to Confocal Microscopy. *Journal of Investigative Dermatology* **2012**, *132* (12), 1–5.

(59) Elliott, A. D. Confocal Microscopy: Principles and Modern Practices. *Current Protocols in Cytometry* **2020**, *92*, e68.

(60) Sperling, R. A.; Parak, W. J. Surface Modification, Functionalization and Bioconjugation of Colloidal Inorganic Nanoparticles. *Philosophical Transactions of the Royal Society A* **2010**, *368* (1915), 1333–1383.

(61) Mahtabani, A.; Rytöluoto, I.; Anyszka, R.; He, X.; Saarimäki, E.; Lahti, K.; Paajanen, M.; Dierkes, W.; Blume, A. On the Silica Surface Modification and Its Effect on Charge Trapping and Transport in PP-Based Dielectric Nanocomposites. *ACS Applied Polymer Materials* **2020**, *2* (8), 3148–3160.

(62) Ying-Mei, X.; Ji, Q.; De-Min, H.; Dong-Mei, W.; Hui-Ying, C.; Jun, G.; Qiu-Min, Z. Preparation of Amorphous Silica from Oil Shale Residue and Surface Modification by Silane Coupling Agent. *Oil Shale* **2010**, *27* (1), 37–46.

(63) Issa, A. A.; Luyt, A. S. Kinetics of Alkoxysilanes and Organoalkoxysilanes Polymerization: A Review. *Polymers* **2019**, *11* (3), 537.

(64) Issa, A. A.; El-Azazy, M.; Luyt, A. S. Kinetics of Alkoxysilanes Hydrolysis: An Empirical Approach. *Scientific Reports* **2019**, *9* (1), 17624–17638.

(65) Labropoulos, A. I.; Romanos, G. E.; Karanikolos, G. N.; Katsaros, F. K.; Kakizis, N. K.; Kanellopoulos, N. K. Comparative Study of the Rate and Locality of Silica Deposition during the CVD Treatment of Porous Membranes with TEOS and TMOS. *Microporous and Mesoporous Materials* **2009**, *120* (1–2), 177–185.

(66) Echeverría, J. C.; Moriones, P.; Arzamendi, G.; Garrido, J. J.; Gil, M. J.; Cornejo, A.; Martínez-Merino, V. Kinetics of the Acid-Catalyzed Hydrolysis of Tetraethoxysilane (TEOS) by 29Si NMR Spectroscopy and Mathematical Modeling. *Journal of Sol-Gel Science and Technology* **2018**, *86*, 316–328.

(67) Sun, S.; Li, H.; Xu, Z. J. Impact of Surface Area in Evaluation of Catalyst Activity. *Joule* **2018**, *2* (6), 1024–1027.

(68) Baetens, R.; Jelle, B. P.; Gustavsen, A. Aerogel Insulation for Building Applications: A State-of-the-Art Review. *Energy and Buildings* **2011**, *43* (4), 761–769.

(69) Vu, A.; Qian, Y.; Stein, A.; Vu, A.; Qian, Y.; Stein, A. Porous Electrode Materials for Lithium-Ion Batteries-How to Prepare Them and What Makes Them Special. *Advanced Energy Materials* **2012**, *2* (9), 1056–1085.

(70) Thomas, A. Much Ado about Nothing – a Decade of Porous Materials Research. *Nature Communications* **2020**, *11* (1), 4985.

(71) Wang, Z.; Yang, J.; Dai, X.; Guo, J.; Li, S.; Sherazi, T. A.; Zhang, S. An Integrated Janus Porous Membrane with Controllable Under-Oil Directional Water Transport and Fluid Gating Property for Oil/Water Emulsion Separation. *Journal of Membrane Science* **2021**, *627*, 119229.

(72) Lei, M.; Qu, X.; Liu, H.; Liu, Y.; Wang, S.; Wu, S.; Bentley, W. E.; Payne, G. F.; Liu, C.; Lei, M.; Qu, X.; Liu, H.; Wang, S.; Liu, C.; Liu, Y.; Wu, S.; Bentley, W. E.; Payne, G. F. Programmable Electrofabrication of Porous Janus Films with Tunable Janus Balance for Anisotropic Cell Guidance and Tissue Regeneration. *Advanced Functional Materials* **2019**, *29* (18), 1900065.

(73) Guan, J.; Gui, H.; Zheng, Y.; You, J.; Li, Y.; Liang, F.; Yang, Z.; Guan, J. P.; Gui, H. G.; Zheng, Y. Y.; Liang, F. X.; Yang, Z. Z.; You, C.; Li, Y. J. Stabilizing Polymeric Interface by Janus Nanosheet. *Macromolecular Rapid Communications* **2020**, *41* (19), 2000392.

(74) Yang, H.-C.; Xie, Y.; Hou, J.; Cheetham, A. K.; Chen, V.; Darling, S. B.; Yang, H.-C.; Darling, S. B.; Xie, Y.; Hou, J.; Cheetham, A. K.; Chen, V. Janus Membranes: Creating Asymmetry for Energy Efficiency. *Advanced Materials* **2018**, *30* (43), 1801495.

(75) Su, H.; Hurd Price, C. A.; Jing, L.; Tian, Q.; Liu, J.; Qian, K. Janus Particles: Design, Preparation, and Biomedical Applications. *Materials Today Bio* **2019**, *4*, 100033.

(76) Zhao, Y.; Sun, M.; Wang, X.; Wang, C.; Lu, D.; Ma, W.; Kube, S. A.; Ma, J.; Elimelech, M. Janus Electrocatalytic Flow-through Membrane Enables Highly Selective Singlet Oxygen Production. *Nature Communications* **2020**, *11*, 6228.

(77) Long, Z.; Zhao, Y.; Zhang, C.; Zhang, Y.; Yu, C.; Wu, Y.; Ma, J.; Cao, M.; Jiang Long, L. Z.; Ma, J.; Jiang, L.; Zhao, Y.; Zhang, C.; Zhang, Y.; Yu, C.; Wu, Y.; Cao, M. A Multi-Bioinspired Dual-Gradient Electrode for Microbubble Manipulation toward Controllable Water Splitting. *Advanced Materials* **2020**, *32* (17), 1908099.

(78) Zhao, Y.; Wang, H.; Zhou, H.; Lin, T. Directional Fluid Transport in Thin Porous Materials and Its Functional Applications. *Small* **2017**, *13* (4), 1601070.

(79) Yan, L.; Yang, X.; Long, J.; Cheng, X.; Pan, D.; Huang, Y.; Shao, L. Universal Unilateral Electro-Spinning/Spraying Strategy to Construct Water-Unidirectional Janus Membranes with Well-Tuned Hierarchical Micro/Nanostructures. *Chemical Communications* **2020**, *56* (3), 478–481.

(80) Zhou, H.; Wang, H.; Niu, H.; Lin, T. Superphobicity/Philicity Janus Fabrics with Switchable, Spontaneous, Directional Transport Ability to Water and Oil Fluids. *Scientific Reports* **2013**, *3*, 2961.

(81) Yang, S.; Yin, K.; Chu, D.; He, J.; Duan, J. A. Femtosecond Laser Structuring of Janus Foam: Water Spontaneous Antigravity Unidirectional Penetration and Pumping. *Applied Physics Letters* **2018**, *113* (20), 203701.

(82) Yong, J.; Chen, F.; Yang, Q.; Huo, J.; Hou, X. Superoleophobic Surfaces. *Chemical Society Reviews* **2017**, *46* (14), 4168–4217.

(83) Yang, X.; Wang, Z.; Shao, L. Construction of Oil-Unidirectional Membrane for Integrated Oil Collection with Lossless Transportation and Oil-in-Water Emulsion Purification. *Journal of Membrane Science* **2018**, *549*, 67–74.

(84) Bolt, G. H. Determination of the Charge Density of Silica Sols. **1957**, *61* (9), 1166–1169.

(85) Předota, M.; Machesky, M. L.; Wesolowski, D. J. Molecular Origins of the Zeta Potential. *Langmuir* **2016**, *32* (40), 10189–10198.

(86) Xie, F.; Nylander, T.; Piculell, L.; Utsel, S.; Wågberg, L.; Åkesson, T.; Forsman, J. Polyelectrolyte Adsorption on Solid Surfaces: Theoretical Predictions and Experimental Measurements. *Langmuir* **2013**, *29* (40), 12421–12431.

(87) Galarneau, A.; Nader, M.; Guenneau, F.; Renzo, F. di; Gedeon, A. Understanding the Stability in Water of Mesoporous SBA-15 and MCM-41. *The Journal of Physical Chemistry C* **2007**, *111*, 8268–8277.

(88) Guthrie, C. P.; Reardon, E. J. Metastability of MCM-41 and Al-MCM-41. *The Journal of Physical Chemistry A* **2008**, *112*, 3386–3390.

(89) Almanza-Workman, A. M.; Raghavan, S.; Deymier, P.; Monk, D. J.; Roop, R. Aqueous Silane-Surfactant Co-Dispersions for Deposition of Hydrophobic Coatings onto Pre-Oxidized Polysilicon. *Colloids and Surfaces A: Physicochemical and Engineering Aspects* **2004**, *232* (1), 67–75.

(90) Anderson, J. L. Colloid Transport by Interfacial Forces. *Annual Review of Fluid Mechanics* **1989**, *21*, 61–99.

(91) Chandler, D. Interfaces and the Driving Force of Hydrophobic Assembly. *Nature* **2005**, *437*, 640–647.

(92) Shaw, D. G.; Maczynski, A.; Goral, M.; Wisniewska-Goclowska, B.; Skrzecz, A.; Owczarek, I.; Blazej, K.; Haulait-Pirson, M.-C.; Hefter, G. T.; Kapuku, F.; Maczynska, Z.; Szafranski, A. IUPAC-NIST Solubility Data Series. 81. Hydrocarbons with Water and Seawater-Revised and Updated. Part 11. C 13-C 36 Hydrocarbons with Water Volume Editors. *J. Phys. Chem. Ref. Data* **2006**, *35* (2).

(93) Shaw, D. G.; Maczynski, A.; Goral, M.; Wisniewska-Goclowska, B.; Skrzecz, A.; Owczarek, I.; Blazej, K.; Haulait-Pirson, M.-C.; Hefter, G. T.; Kapuku, F.; Maczynska, Z.; Szafranski, A. IUPAC-NIST Solubility Data Series. 81. Hydrocarbons with Water and Seawater-Revised and Updated. Part 10. C 11 and C 12 Hydrocarbons with Water Volume Editors. *J. Phys. Chem. Ref. Data* **2006**, *35* (1).

(94) Maczynski, A.; Shaw, D. G.; Goral, M.; Wisniewska-Goclowska, B.; Skrzecz, A.; Owczarek, I.; Blazej, K.; Haulait-Pirson, M.-C.; Hefter, G. T.; Kapuku, F.; Maczynska, Z.; Szafranski, A.; Young, C. L. IUPAC-NIST Solubility Data Series. 81. Hydrocarbons with Water and Seawater-Revised and Updated. Part 5. C 7 Hydrocarbons with Water and Heavy Water Volume Editors. *J. Phys. Chem. Ref. Data* **2005**, *34* (3).

(95) Shaw, D. G.; Maczynski, A.; Goral, M.; Wisniewska-Goclowska, B.; Skrzecz, A.; Owczarek, I.; Blazej, K.; Haulait-Pirson, M.-C.; Hefter, G. T.; Huyskens, P. L.; Kapuku, F.; Maczynska, Z.; Szafranski, A. IUPAC-NIST Solubility Data Series. 81. Hydrocarbons with Water and Seawater-Revised and Updated. Part 9. C 10 Hydrocarbons with Water Volume Editors. **2006**.

(96) Morgado, P.; Ao Barras, J. ~; Duarte, P.; Filipe, E. J. M. Solubility of Water in N-Alkanes: New Experimental Measurements and Molecular Dynamics Simulations. **2019**.

(97) Morgado, P.; Barras, J.; Galindo, A.; Jackson, G.; Filipe, E. J. M. Solubility of Water in Mixtures of (n-Alkanes + n-Perfluoroalkanes) and in n-Perfluoroalkylalkanes: Experiments and Modelling with the SAFT-γ Mie Group-Contribution Approach. *https://doi-org.proxy.library.uu.nl/10.1080/00268976.2021.1910743* **2021**, *119* (15–16), 15–16.

(98) Kawamura, A.; Takai, C.; Fuji, M.; Shirai, T. Effect of Solvent Polarity and Adsorbed Water on Reaction between Hexyltriethoxysilane and Fumed Silica. *Colloids and Surfaces A: Physicochemical and Engineering Aspects* **2016**, *492*, 249–254.

8. Appendices

Appendix 1: Lamda scan of 2 untreated, fresh fibers. The average was used to normalize the data in Figure 20.

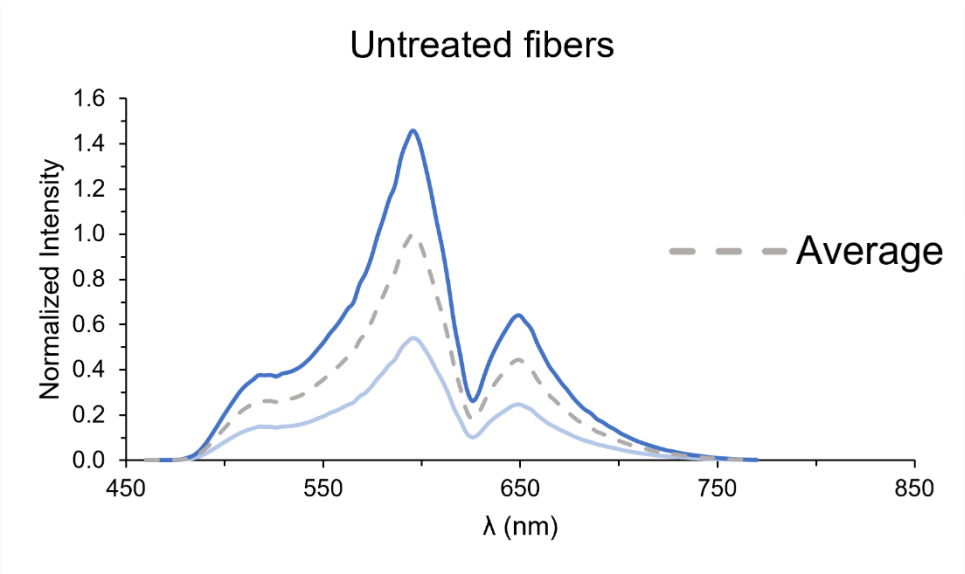

Appendix 2: During spectral scans the ROI was set to a section of the fiber to selectively monitor fluorescence response of bijel fibers.

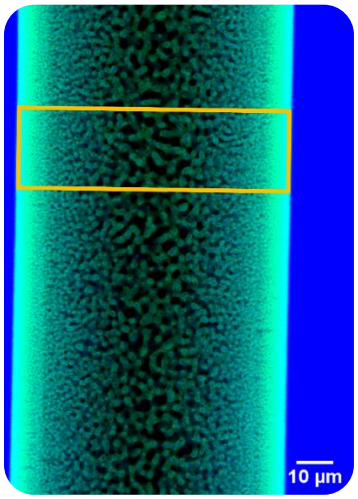

Appendix 3: Image processing in ImageJ

The contrast could be adjusted by going to "*Image > > Adjust >> Brightness/Contrast*". These were edited as described in section 3.10.

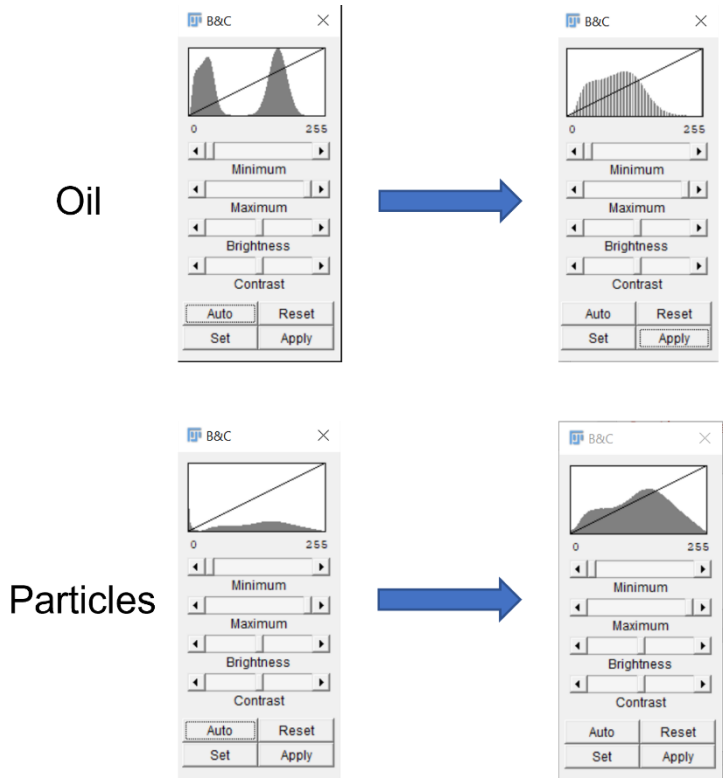

The color channels were merged by clicking "*Image > > Color >> Merge Channels*" and selecting blue for the oil channel and green for the particle channel. A scalebar was added at "*Analyze > > Tools >> Scale Bar…*".

Appendix 4: Confocal micrographs of fibers for different TEOS concentrations and reaction times. For each set the fibers were washed (*OCTANOL*) an unwashed (INTACT) reference micrographs were recorded. Importantly, most fibers contained oil-to-water channel leakage. We imaged mainly the intact fibers, as these could be use for the spectral scans to assess the amount of CTAB.

8h-3%-OCTANOL	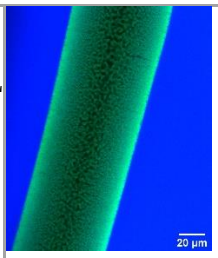	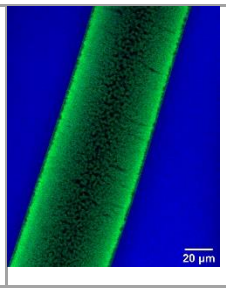	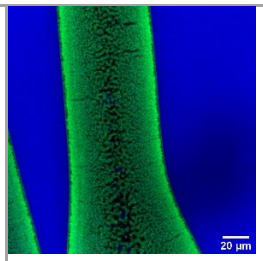	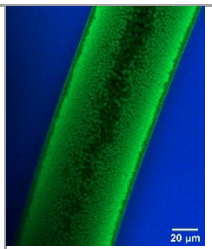

8h-3%-INTACT	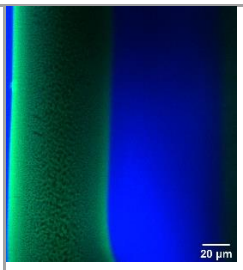	V 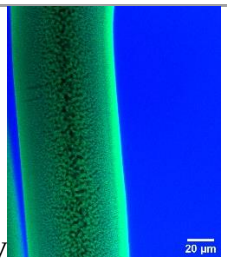		
8h-5%-OCTANOL	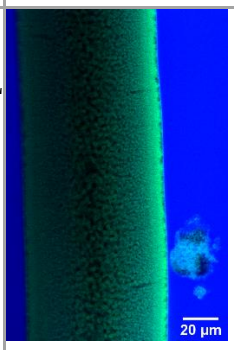	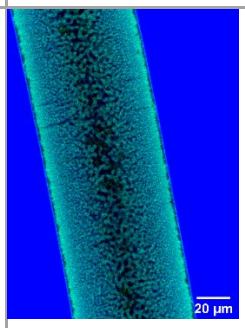		
8h-5%-INTACT	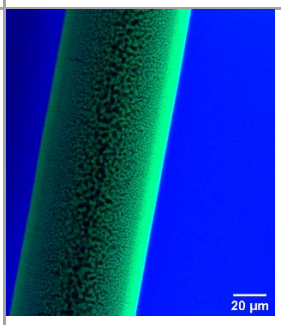	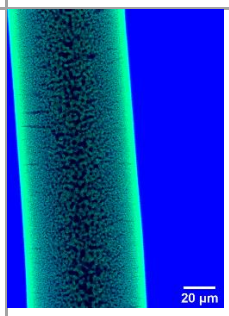		
18h-1%-OCTANOL	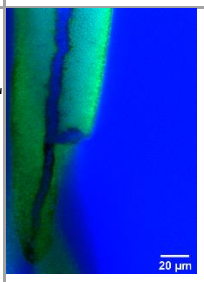	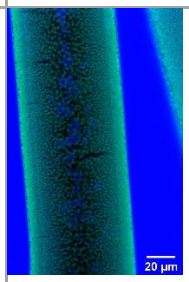	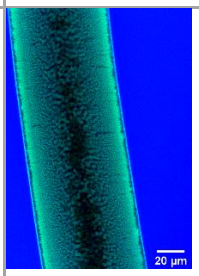	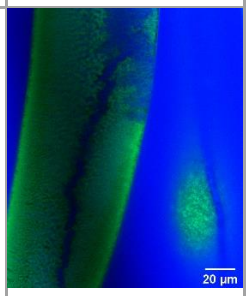
18h-1%-INTACT	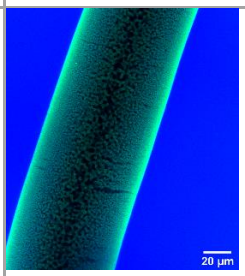	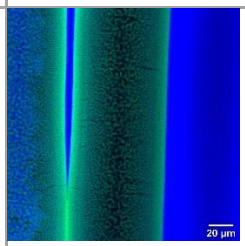		
18h-3%-OCTANOL	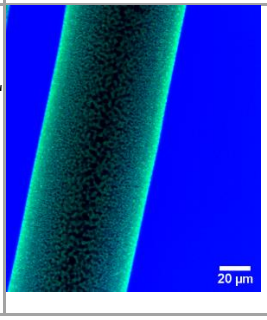	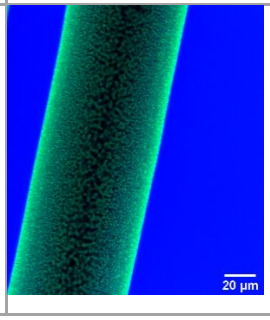	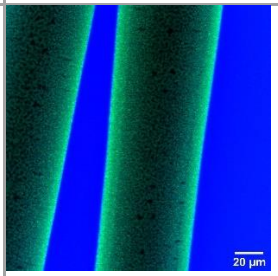	

18h-3%-INTACT	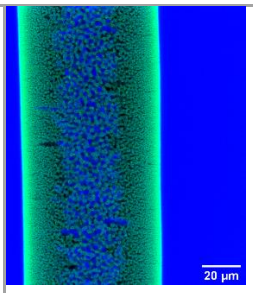	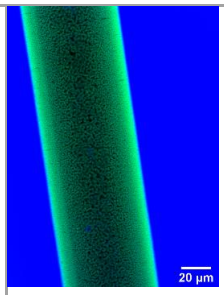	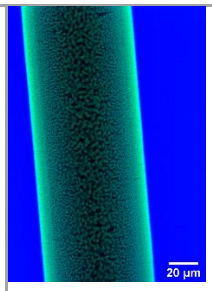	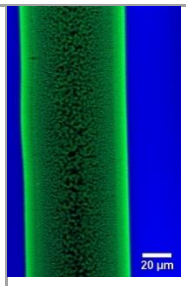
18h-5%-OCTANOL	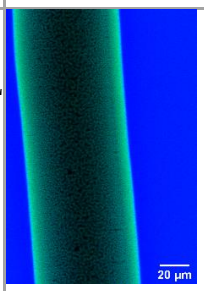	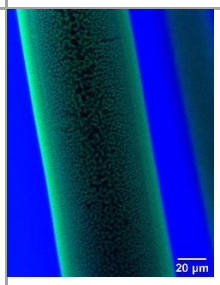		
18h-5%-INTACT	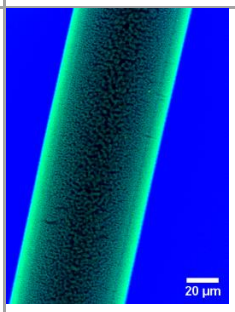	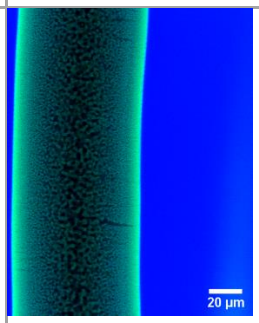		
75h-1%-OCTANOL	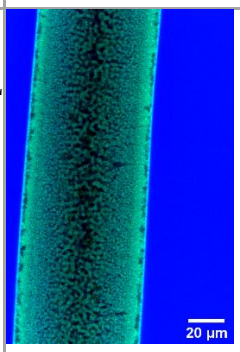	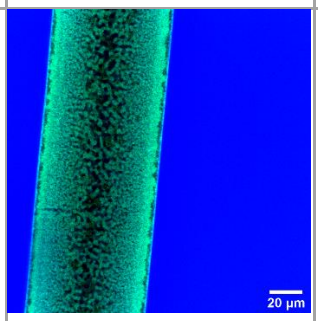		
75h-1%-INTACT	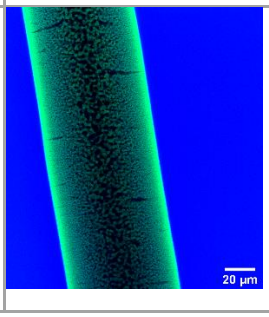	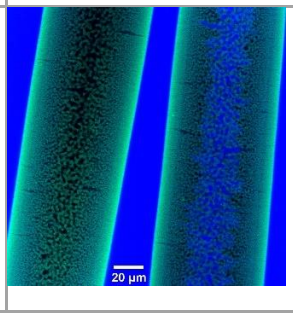	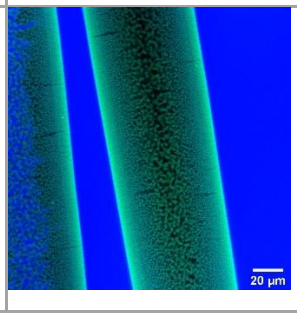	

75h-3%-OCTANOL	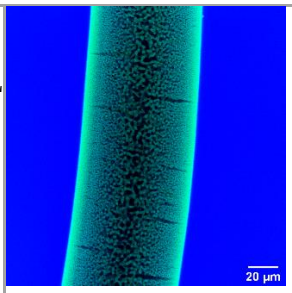	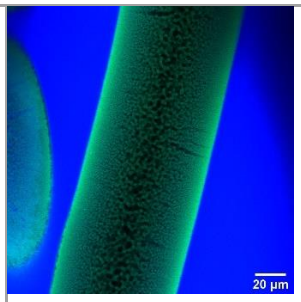		
75h-3%-INTACT	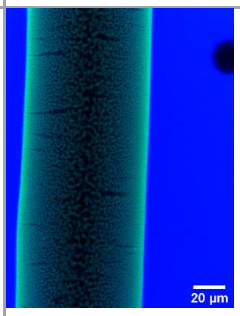	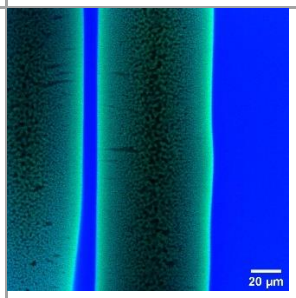		
75h-5%-OCTANOL	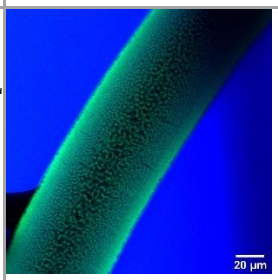	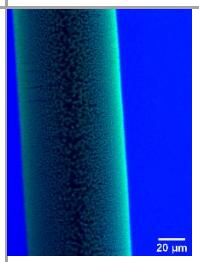		
75h-5%-INTACT	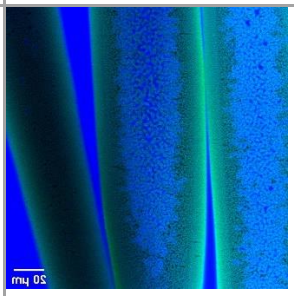	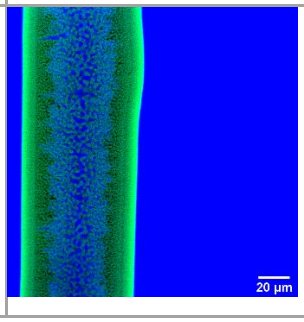		

Appendix 5: Spectral scans of octanol washed fibers for different TEOS-treatment strengths. *Octanol* means the fibers were washed once, *Intact* means they were unaltered.

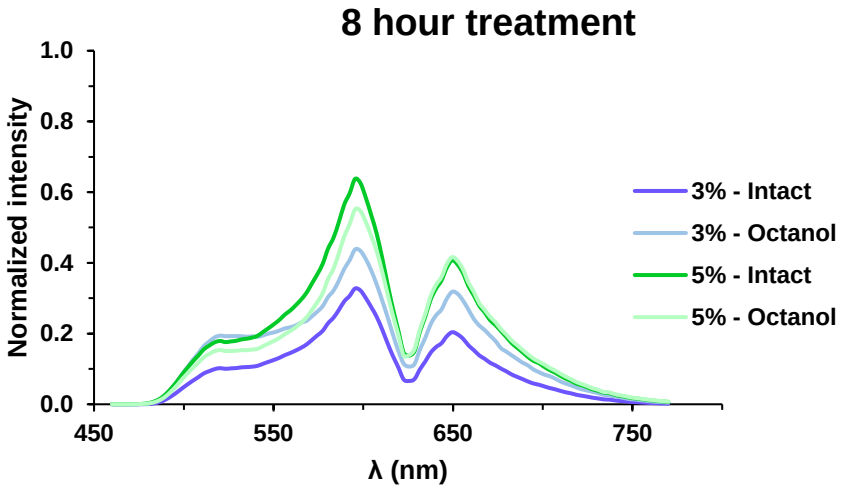

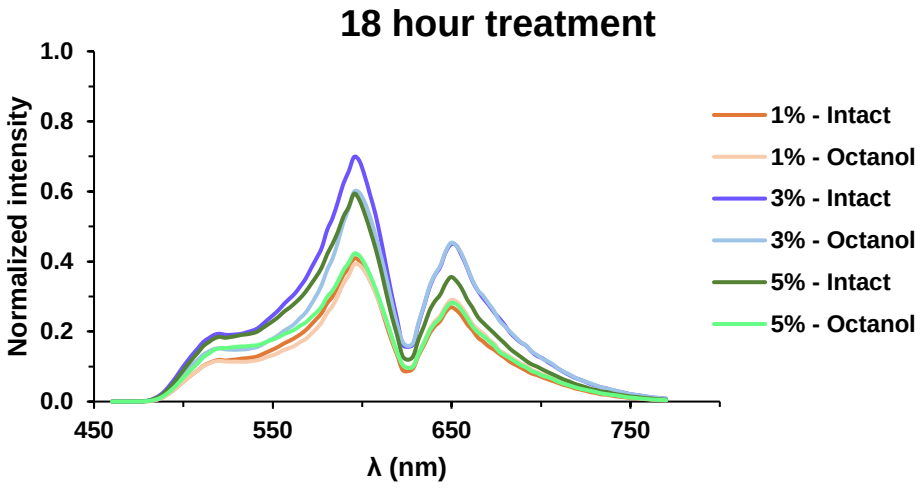

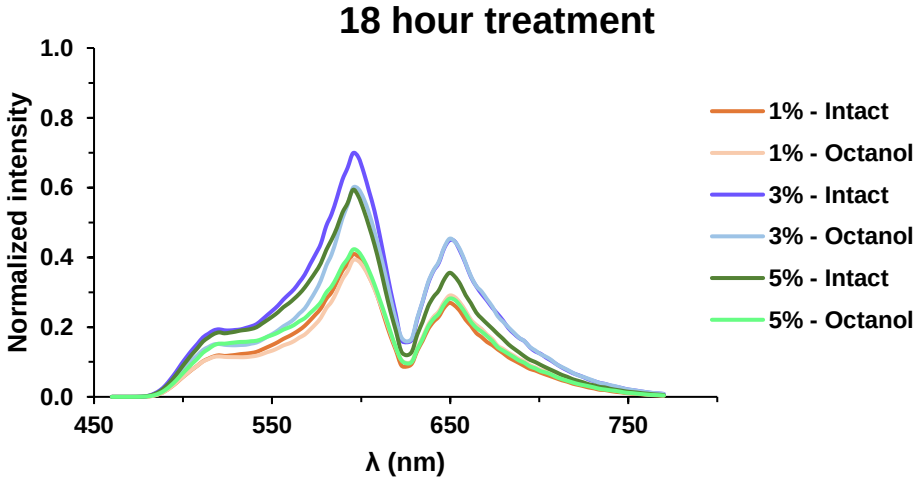

Appendix 6: Spectral scans of octanol washed fibers for the indicated number of steps. All fibers were TEOS treated for 18 hours.

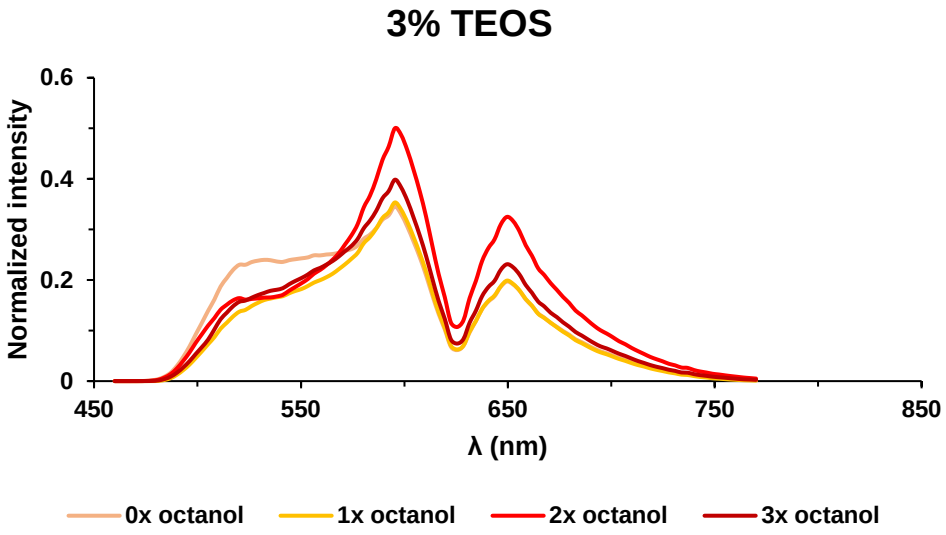

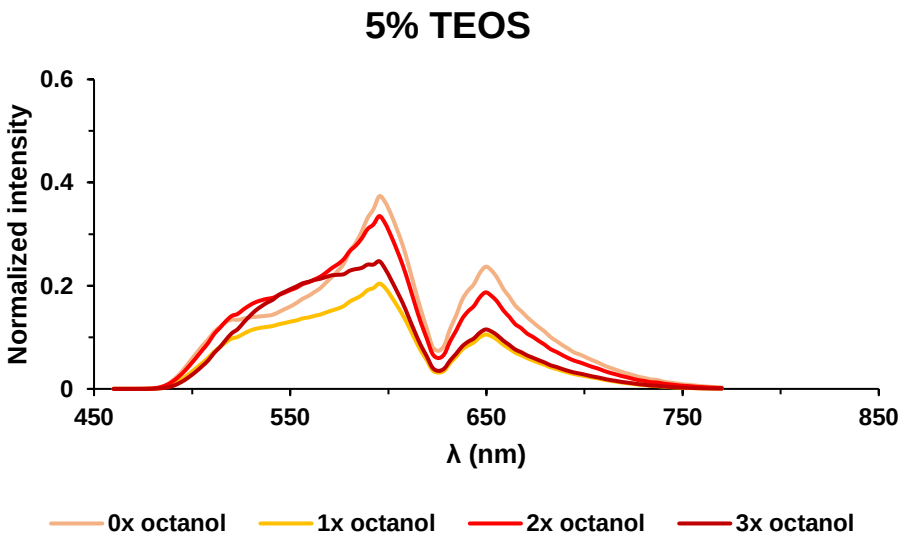

Appendix 7: Determining oil and water content of fibers

We adapted dr. M.F. Haase's procedure for finding the interfacial area to calculate the volume fraction of oil in the bijel. We only used the micrograph of the oil channel. The contrast was increased in ImageJ and an FFT bandpass filter was applied. We set a threshold and converted the image to a binary format so it could be used for analysis. The oil phase is shown in white and the water channel in black.

The image was rotated so the fiber pointed straight up. The white region outside the fiber does not contain any information about the fiber and was removed. Unfortunately the thresholding

made the pores close to the surface black. Black means water, so counting these would falsely increase the overal water fraction. The image was cropped such that only the bicontinuous interior was kept.

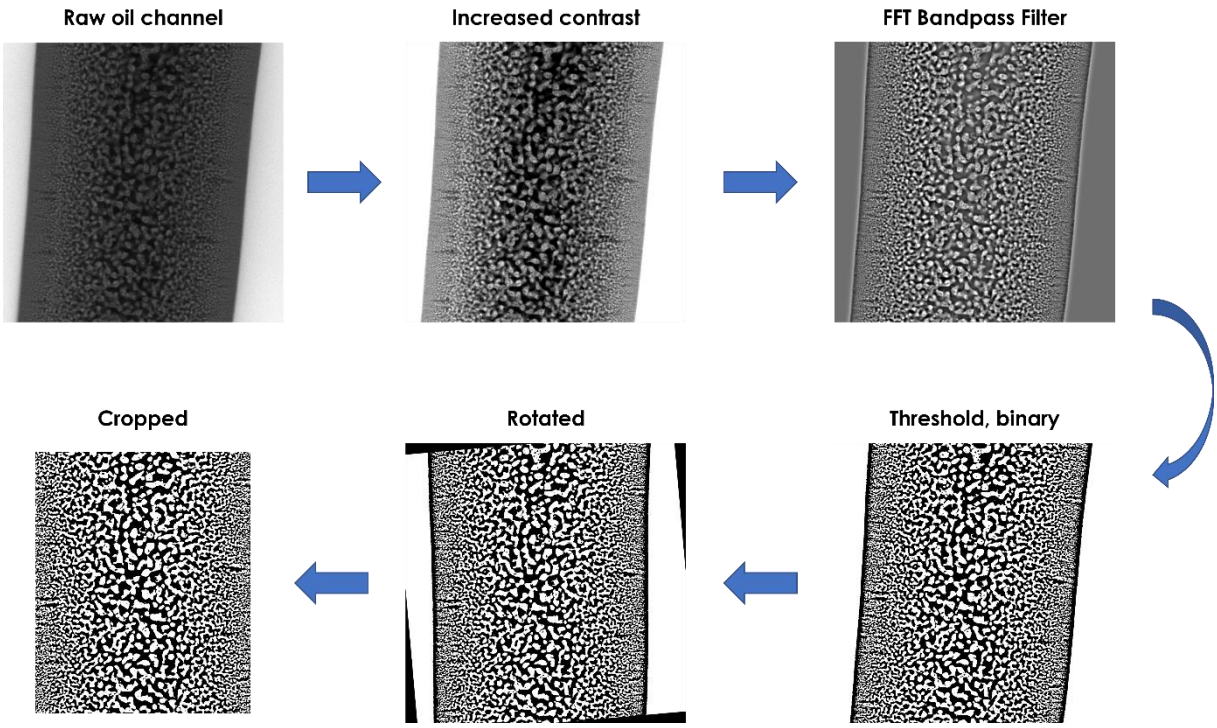

The image was split at the fiber center, creating two images.

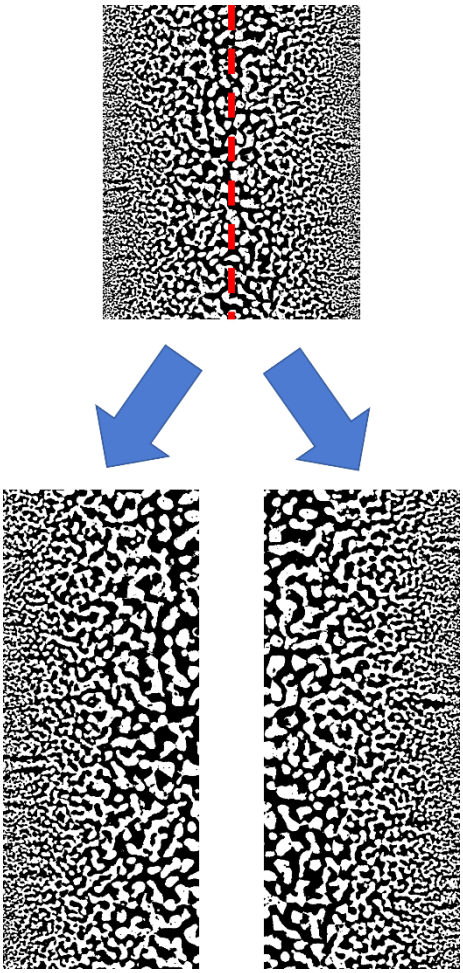

Under "*Analyze >> Set Measurements…*" the boxes of "*Area*" and "*Limit to threshold*" were selected.

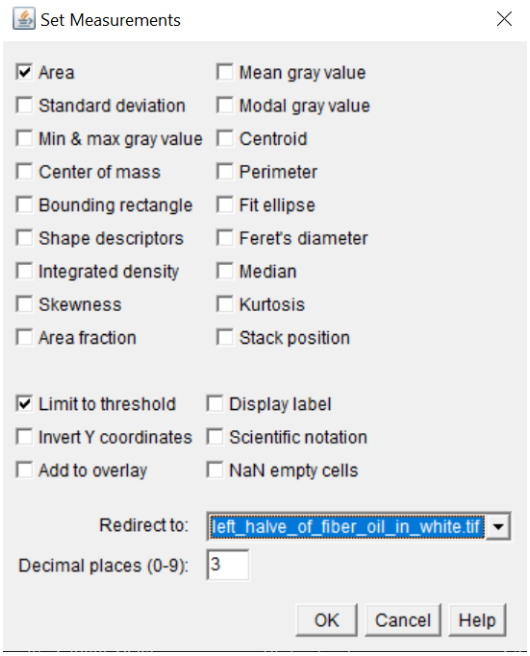

Unfortunately we could not simply add up the white pixels from this image to get the oil volume. It is a cross-section at the center of the fiber. The fact that the fibers are cylindrical means that the parts further from the center have a larger contribution to the volume of the fiber.

Because of this cylindrical shape there should be a factor $2\pi r$. The first step to do this was to devide the image into rectangular parts. We wrote a short Matlab script to do this repetitive task:

```
clear all
clc

x_pixels = 614; %enter here the x-width of the image
y_pixels = 1746;

x_pixels_var = x_pixels - 1; %takes out the right black border from analysis
y_pixels_var = y_pixels - 2; %y_length after subtracting the borders

for n = 2:x_pixels_var %starts at 2 to remove the left black border
 ret = 'makeRectangle(%u, 1, 1, %u);\nrun("Measure");\n'; %starts at 2 to remove the top left border from analysis
 % assigns variables n and y_pixels_var, respectively. ('makeRectangle(x, y, x_width, y_width)
 fprintf(ret, n, y_pixels_var);
end
```

Matlab then prined iterations of the lines:

"*makeRectangle(x, y, 1, [Y]);*

run("Measure");"

[Y] is a measure for the number of pixels in the y-direction.

When this Matlab output was run in ImageJ it created a rectangle of 1 x [Y] pixels. ImageJ automatically made the borders of the image black, so we made sure these were not incorporated.
The second line subsequently measured the number of the white pixels.

The code was executed in ImageJ by going to "*Plugins* > > *Macros* >> *Record…*" The output of the Matlab file was copied to here and a .ijm file with the code was created by clicking on "*Create*". "*Run*" returned a table with the results.
These could be saved as a .csv file and opened in Excel. The first column gives the radius in pixels, which was converted to µm. The volumes were calculated using the formula:

$$V_x = A_x \cdot 2\pi \cdot r$$

Where V_x and A_x are the volume and area of phase-x. r is the distance from the center.

Adding up all volume slices should give such an output:

radius pixels)	radius(µm)	Area (µm^2)	MinThr	MaxThr	volume (µm^3)
1	0,050480065	2,26	255	255	0,717594
2	0,100960131	2,204	255	255	1,399626
3	0,151440196	2,148	255	255	2,046096
4	0,201920262	2,163	255	255	2,74718
5	0,252400327	2,107	255	255	3,345069
6	0,302880393	2,123	255	255	4,044565
7	0,353360458	2,24	255	255	4,978708
8	0,403840523	2,332	255	255	5,923646
9	0,454320589	2,357	255	255	6,735544
10	0,504800654	2,421	255	255	7,68715
11	0,55528072	2,449	255	255	8,553661

	Oil volume (µm^3)	Water volume (µm^3)
left half	188140,9207	216219,8035
right half	194709,5311	208563,564
Total	*382850,4518*	*424783,3675*
Fraction	0,474039648	0,525960352

Appendix 8: Calculation of water volume

$$V_{aq} = V_{H_2O} + (V_{LUDOX} - V_{particles})$$

The total volume of the water is the water volume plus the volume of the LUDOX TMA stock minus the particle volume.

$$V_{particles} = N_{particles}\, v = \frac{m_{tot,p}}{m_p} v$$

$N_{particles}$ is the number of particles and v is the volume per particle, r the particle radius (10 nm) $m_{tot,p}$ is the mass of all particles and m_p is the mass of a single particle.

Mass as an expression of the weight fraction w and the total mass m_{tot}:

$$m = w m_{tot} = w \rho V$$

Combining these two leads to the equation, and filling it in for a ternary volume of 2 mL:

$$V_{particles} = \frac{w\rho_{stock}V_{stock}}{\rho_{SiO_2}v}v = \frac{w\rho_{stock}V_{stock}}{\rho_{SiO_2}} = \frac{0.45 \cdot 1.26\,\frac{g}{mL} \cdot 0.868\,mL}{2.65\,\frac{g}{mL}} = 0.19\,mL$$

This results in a total volume

$$V_{aq} = 0.132\,mL + (0.868\,mL - 0.19\,mL) = 0.81\,mL$$

Resulting in a volume fraction of water φ_{H_2O}

$$\varphi_{H_2O} = \frac{V_{H_2O}}{V_{ternary}} = \frac{0.81\,mL}{2\,mL} = 0.41$$

We flow ternary at 0.5 mL/h for 2 minutes per container. The total volume of water V_{H2O} can be expressed in the flow rate Q and the time t.

$$V_{H_2O} = \varphi_{H_2O}Qt = 0.41\ \cdot 0.5\,\frac{mL}{h} \cdot 2\,\frac{min}{60\,\frac{min}{h}} = 6.8\,\mu L$$

In 2 mL of dodecane this results in a mole fraction x_{H2O} of

$$x_{H_2O} = \frac{n_{H_2O}}{n_{tot}} = \frac{\rho_{H_2O}V_{H_2O}M_{dod}}{M_{H_2O}\rho_{dod}V_{dod}} = \frac{0.997\,\frac{g}{mL} \cdot 6.8 \cdot 10^{-3}\,mL \cdot 170.33\,\frac{g}{mol}}{18.02\,\frac{g}{mol} \cdot 0.750\,\frac{g}{mL} \cdot 2\,mL} = 4.2\ \cdot 10^{-2}$$

This is well above the maximum solubility $x_{H2O} = 6.1 \cdot 10^{-4}$. However, this is for the entire water phase. This is not what actually happens, since only a small amount dissolves at one time. The displaced water could be deposited elsewhere in the fiber, such that the concentration never actually increases above the maximum solubility.

Appendix 9: For reconstitution experiments of hydrophobized fibers, references were used which were rewetted with only oil, or only water. In both cases the dye was drained from the liquid due to strong adsorption to the particles, and no fluorescence signal was recorded in the liquid. For the water reference, the gain was increased to almost 100%. The signal is not actually the water channel, but the tail-end of the particle fluorescence at lower wavelengths. This can be seen since the two signals overlap exactly.

	Fiber rewetted with:	
Fluorescence channel	Oil	Water
Particles	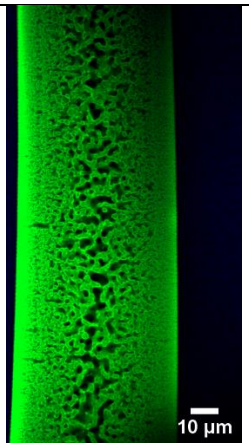	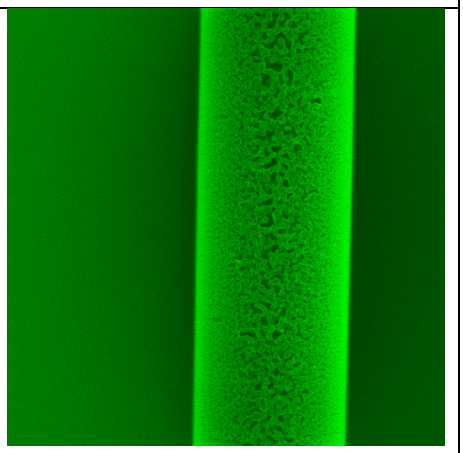
Water	-	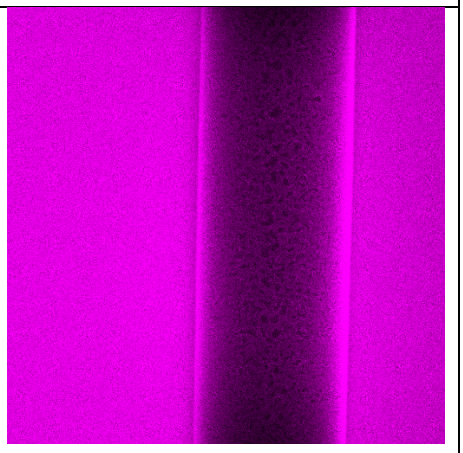

Oil	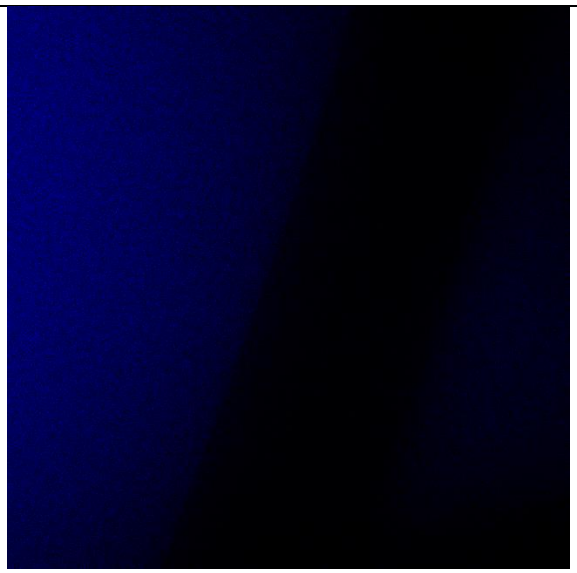	-

Appendix 10: Comparison of hydrophobized fibers pre- and post drying. The gain had to be increased drastically to record some signal for OTS treated fibers, and no fluorescence was recorded at all after drying. The dye could hardly penetrate the thick residue on the fiber.

	Pre-drying	**Reconstituted**
OTS	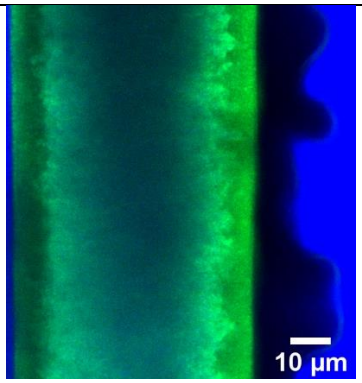	No fluorescence signal
HTES	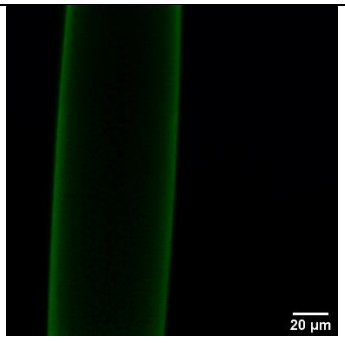	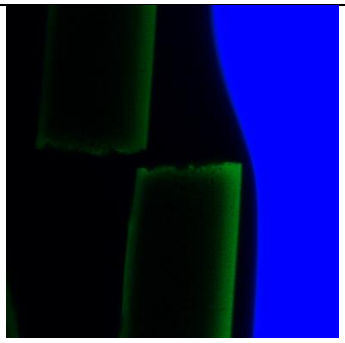

Appendix 11: SEM micrograph of an octanol washed fiber treated with 5% HTES.